Student thesis series INES nr 492

Conceptualizing green water within the planetary boundary for freshwater use

Arne Tobian

2019
Department of
Physical Geography and Ecosystem Science
Lund University
Sölvegatan 12
S-223 62 Lund
Sweden

Arne Tobian (2019).
Conceptualizing green water within the planetary boundary for freshwater use

Master degree thesis, 30 credits in Physical Geography and Ecosystem Analysis
Department of Physical Geography and Ecosystem Science, Lund University

Level: Master of Science (MSc)

Course duration: September 2018 until January 2019

Disclaimer

Conceptualizing green water within the planetary boundary for freshwater use

---

Arne Tobian

Master thesis, 30 credits, in Physical Geography and Ecosystem Analysis

Supervisors:
Prof. Dieter Gerten, Potsdam Institute for Climate Impact Research (PIK), RD1: Earth System Analysis

Prof. Anna Maria Jönson, Lund University,
Department of Physical Geography and Ecosystem Sciences

Exam committee:
Stefan Olin, Lund University,
Department of Physical Geography and Ecosystem Sciences

Adrian Gustafson, Lund University,
Department of Physical Geography and Ecosystem Sciences

Abstract

Anthropogenic land-use covers a constantly increasing fraction of the terrestrial surface area. By employing a dynamic global vegetation model, human-induced changes in the terrestrial water balance as compared to an undisturbed scenario were simulated. The results suggest that humanity is a main driver of change in the terrestrial water balance in general and green water in particular. Most striking is the shift from biophysical plant transpiration to purely physical soil evaporation caused by deforestation. This intervention into the terrestrial water vapor flux has strong implications for regional and continental moisture recycling and can contribute towards reaching potential tipping points in the Earth system. All things considered, this study evaluates a qualitative and quantitative fundament of accounting for green water within the Planetary Boundary for Freshwater use to help preventing detrimental and unacceptable human interferences with the terrestrial water cycle.

Keywords: Green water · Planetary boundary · Water stress · Land-use · Moisture recycling · Land use modelling · Evapotranspiration · Earth system · Potential natural vegetation

Contents

1. Introduction 1
2. Background 2
2.1 A safe operating space for humanity 2
2.2 The Planetary Boundary for Freshwater use 3
2.2.1 Current definition of the Planetary Boundary for Freshwater use 3
2.2.2 Critique of the definition 4
2.3 Green water - the birth of a terminology 5
2.3.1 Demarcating between blue and green water 5
2.3.2 Green water availability, deficiency and scarcity 7
2.4 Green water in the Earth System 8
2.4.1 The role of green water for biophysical processes 8
2.4.2 Moisture recycling and precipitationsheds 9
2.4.3 Green water – climate interaction 10
2.4.4 Green water related tipping points in the earth system 11
2.5 Anthropogenic changes in green water 12
3. Methods 15
3.1 The LPJmL Model 15
3.1.1 Model description and justification 15
3.1.2 Terrestrial water balance in LPJmL 16
3.2 Simulation protocol 16
3.3 Measuring green water 18
3.4 Data processing and visualization 19
4. Results 20
4.1 Globally aggregated values 20
4.2 Global maps 22
4.2.1 Deforestation and irrigation changes on GW-flow 22
4.2.2 Changes in GW availability, GW_{eff} and L_{TA} 22
4.3 Regional plots 25
5. Discussion 26
5.1 The concept of green water 26
5.2 Results of the modelling study 27
5.3 Implementing green water in the Planetary Boundary for Freshwater use 30
5.3.1 The green gap 30
5.3.2 A green water-based control variable 31
6. Conclusions and outlook 34
References 35
Appendix 42

List of acronyms and abbreviations

ALC	Anthropogenic land-cover
ALCr	Simulation run with anthropogenic land-cover
ALCr_irr	Simulation run with anthropogenic land-cover and irrigation schemes
BW	Blue Water
CFT	Crop functional type
CV	Control Variable
ES	Earth System
GW	Green Water
GW_{eff}	Green Water flow efficiency index
GW-flow	Green Water flow
LPJmL	Lund-Potsdam-Jena with managed Land
L_{TA}	Water limitation index
MIPs	Most influential precipitationsheds
PB	Planetary Boundary
PB-W	Planetary Boundary for Freshwater use
PFT	Plant functional type
PNV	Potential natural vegetation
PNVr	Simulation run with potential natural vegetation

List of figures

Figure 1. Planetary boundaries framework 2
Figure 2. Water color scheme 7
Figure 3. Precipitationshed draft 10
Figure 4. Impacts of human activity on the moisture recycling feedback 14
Figure 5. Simulation protocol 17
Figure 6. Sum of all positive and negative changes for various GW-related parameters 21
Figure 7. Deforestation and irrigation GW-flow changes 22
Figure 8. GW availability, GW_{eff} and L_{TA} 23
Figure 9. Global distribution of PFTs and CFTs under ALCr_irr 25
Figure 10. Intra-annual trends of GW_{avail}, E_{soil} and E_{transp} 25
Figure 11. Updated Planetary Boundaries framework 32
Figure 12. GW_{eff} -based preliminary draft of a subglobal control variable 33

List of tables

Table 1. Overview of green and blue water related terms and their definitions 8
Table 2. Green water related tipping elements 11
Table 3. Simulation run set-ups and descriptions 17
Table 4. Global values of GW-related parameters 20

1. Introduction

Ever since the beginning of the industrial revolution, increasing socio-economic demands and activities have exerted an unprecedented and constantly increasing anthropogenic pressure on the interfering physical, biological and chemical processes, cycles and spheres of the earth system (ES). Especially after the second half of the 20th century, when socio-economic trends, among others water consumption, population growth or GDP, steeply accelerated, the manifold environmental stress indicators, such as atmospheric CO_2 concentration or terrestrial biosphere degradation, started to simultaneously show a steep aggravation. This interlinked phenomenon has been coined as the 'Great Acceleration' (Steffen et al. 2004; Steffen et al. 2015a) and emphasizes the necessity of a holistic and science-based framework of the biophysical limits of the ES. In fact, a continuously boundless exploitation would risk the stability and well-functioning of planet earth in such a scale that we would risk leaving the Holocene-like stadium, the only ES-stadium that we know that humanity can prosper and thrive in (Steffen et al. 2011). Rockström et al. (2009c) postulated the Planetary Boundary framework. By identifying and quantifying nine distinct but partly interdependent 'Planetary Boundaries' (PB) for human interference with critical ES processes, the PB framework aims at constituting the scientific basis for guiding global sustainable development in the Anthropocene. Within the context of the scientific endeavor to constantly query and enhance the framework, the Planetary Boundary for Freshwater use (PB-W) has constantly been subject to review and refinement (Molden 2009; Gerten et al. 2013; Jaramillo and Destouni 2015; Gerten et al. 2015; Heistermann 2017). Recently, there has been vehement criticism that a crucial aspect of the terrestrial water cycle, namely the often overlooked green water has not yet been adequately accounted for within PB-W (Heistermann 2017). Green water plays a central role in the ES. In the context of human prosperity, green water is of vital value and constantly appropriated to produce food and commodities. To illustrate, it has been estimated that a grand of 5,000 km³ yr^{-1}, out of the 6,800 km³ yr^{-1} water being consumed for agricultural production stem from rain replenished green water (Falkenmark and Rockström 2006). This number is backed up by the fact that 80% of agricultural land (Falkenmark and Rockström 2006) and 60% of staple food production (Savenije 2000) rely on rainfed, thus green water-based, agriculture. Against the backdrop of future challenges in food and freshwater provision for an ever-growing world population, accounting for green water within the guidelines of global sustainable development seems vital (Rockström et al. 2014).

This thesis aims at conceptualizing the qualitative and quantitative fundaments of green water within PB-W and thereby at closing the conceptual research gap (Jaramillo and Destouni 2015; Gerten et al. 2015; Heistermann 2017). First, the vital role of green water for biophysical processes and tipping points in the ES will be elaborate with a literature study. Second, human interferences with the terrestrial water cycle will be simulated and quantified with the help of a global dynamic vegetation and water balance model. In this regard, global and regional analyses will highlight the complex interaction between human activity and green water. Finally, the derived understanding of changes in green water will build the basis to conceptualize green water within the Planetary Boundary for Freshwater use.

2. Background

2.1 A safe operating space for humanity

The Planetary Boundary framework, introduced by Rockström et al. (2009c) and updated by Steffen et al. (2015b) tries to fill the paradigmatic gap of a holistic and science-based guideline for human development by defining a safe operating space for humankind (figure 1).

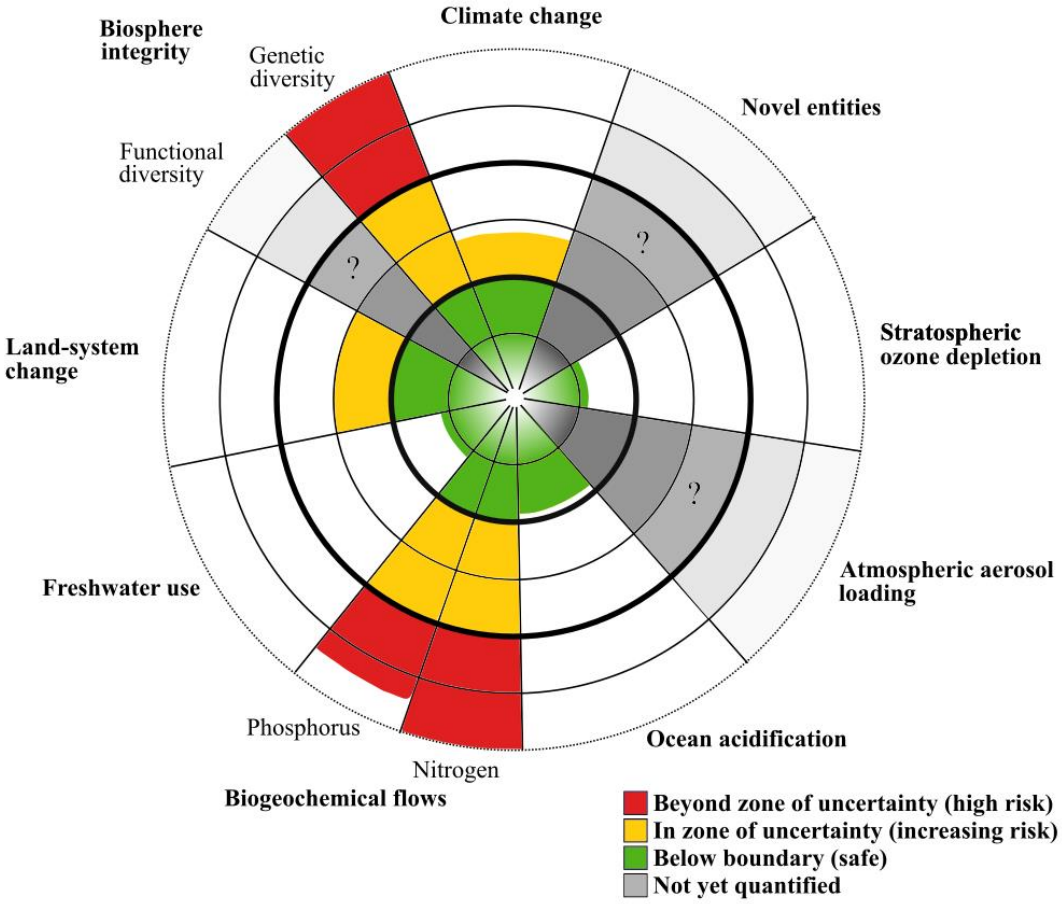

Figure 1. Planetary boundaries (PB) framework. The Earth system is split into nine individual PBs and the current state of each PB boundary is based on the status of its respective control variable(s). At the lower end of uncertainty (within the inner bold circle), lays the safe operating space for humanity. The upper end of uncertainty, in turn, implies a dangerous interference (outside the outer bold circle). Based on and adapted from Steffen et al. (2015b).

The adjunct 'safe' refers hereby to assure staying within the Holocene-like stadium and is based on the precautionary principle, constituting a guideline for environmental policy related decision making (Kriebel et al. 2001; Rockström et al. 2009b). In the context of the PB framework, the precautionary principle finds its manifestation in the fact that each boundary is set at the lower end of the respective uncertainty zone, leaving a margin towards reaching potential biophysical thresholds (yellow 'zone of uncertainty' in figure 1). One or more control variables (CV) act hereby as numerical target values monitoring the current status of each respective PB and determine the physical limits of human intervention in the respective aspect

of the ES. It is thus paramount that CVs are defined to cover the related biogeochemical and physical processes behind a respective PB as ample as possible. Exceeding PBs and subsequently approximating potential thresholds, thus non-linear and potentially irreversible transitions, would set the ES stability at risk and consequentially be detrimental to human prosperity (Lenton et al. 2008). The central question is to what extent the PB framework is capable of monitoring dangerous anthropogenic interferences with the ES.
Identifying and quantifying thresholds and suitable CVs is thus a fundamental challenge within the PB framework. Another challenge arises from understanding and depicting the interdependency of different PBs, for example, how transgressing the Planetary Boundary for Freshwater use could affect the status of Planetary Boundary of Climate Change and vice versa. Since its origination in 2009, the PB framework has undergone vast scientific scrutiny (Allen 2009; Molden 2009; Lewis 2012; Heistermann 2017) and triggered debates far beyond the scientific community.

2.2 The Planetary Boundary for Freshwater use

By building dams, straightening and regulating the course of entire river systems and by withdrawing water for irrigation, humankind has become the dominant force of change in riverine and freshwater systems on a planetary scale with tremendous consequences for river streamflow (Meybeck 2003). Based on the concept of the PB framework, an upper limit of freshwater consumption has been defined in PB-W in order to sustain the well-functioning of interlinked ES processes.

2.2.1 Current definition of the Planetary Boundary for Freshwater use

The total stock of surface waters (including river discharge, lakes and reservoirs) and refreshable groundwater stores will hereby be referred to as blue water (BW). Currently, the PB-W is defined as the upper limit of consumptive BW use to avoid severe damages to the ES (Falkenmark and Rockström 2004; Rockström et al. 2009b; Steffen et al. 2015b). It has been seen by Rockström et al. (2009b) that consumptive BW use is a sufficiently capable proxy for human interventions with the entire terrestrial water cycle (detailed justification in the supplementary information of Rockström et al. 2009b). Critique of this simplified approach will be elucidated in the subsequent chapter 2.2.2. Subsequently, the status of interference with BW resources is monitored by two CVs operating on two different spatial scales global and subglobal (river-basin-based), respectively.

The positioning of the global CV for consumptive BW use is based on the premise that if more than 4,000 $km^3\ yr^{-1}$ (that is the lower end of the 4,000-6,000 $km^3\ yr^{-1}$ uncertainty margin) of the 12,500-15,000 $km^3\ yr^{-1}$ available BW (de Fraiture and Wichelns 2010) is being consumed, irreversible changes to terrestrial and aquatic ecosystems will be unavoidable. Such irreversible changes encompass, among others, the collapse of river, estuary, coastal and limnic ecosystems (Rockström et al. 2009b).

Proposed by Gerten et al. (2013), the bottom-up river-basin scaled CV accounts for spatially and seasonally explicit minimum environmental flow requirements to maintain a healthy ecological state of the respective basin that the global CV is not suitable to resolve. By doing so, they calculated an uncertainty margin of 1100-4500 $km^3\ yr^{-1}$ as a global aggregate of subglobal consumptive BW use. Withdrawing more BW from a river than its minimum requirements, for example to irrigate adjacent agricultural land, can threaten the ecosystem state of the respective basin. Nevertheless, the lower end of the uncertainty margin is substantially lower than the currently estimated globally aggregated usage of BW, pointing towards local to regional transgressions of the PB-W.

Albeit the global CV of the PB-W as proposed by Rockström et al. (2009b) retained unchanged in the updated version of the PB framework, the additional river basin-scale CV as proposed by Gerten et al. (2013) has be introduced to complement the PB-W by making subglobal transgressions visible within the PB framework (Steffen et al. 2015b).

2.2.2 Critique of the definition

Regarding the global CV:
The current value of the global CV is ~2,600 $km^3\ yr^{-1}$ and accordingly well below the critical value of 4,000 $km^3\ yr^{-1}$ (Steffen et al. 2015b), thereby conveying the impression that humanity is well within a safe operating space in terms of global water consumption. On the one hand this number has been challenged by Molden (2009), highlighting that local conditions and water managements strategies are not factored in. On the other hand, uncertainty margins are not only defined by uncertainties in the response of the ES but also within the given numbers. To illustrate, global runoff withdrawal estimations depend highly on contemporary water use statistics which are often compiled on a national level and prone to be outdated. As a consequence, estimations vary substantially at about ~1,300 $km^3\ yr^{-1}$ (Vörösmarty et al. 2000 and references therein).

Regarding the river-basin-based CV:
The current status of the CV has been challenged by Jaramillo and Destouni (2015). On the one hand they argue that the current value of ~2600 $km^3\ yr^{-1}$ is based on outdated estimations and that updated reservoir-related estimations were ignored in the updated assessment of the PB-W by Steffen et al. (2015b), implying that the set PB-W potentially has been transgressed on a global level. On the other hand, they point out that focusing on BW alone is an insufficient representation of the water cycle. Instead, they argue, anthropogenic changes of green water (GW) processes due to anthropogenic land-cover (ALC) must be accounted for in order to represent a holistic view of the water cycle and human perturbations. In sum, they conclude, consumptive freshwater use accounts for 4,664 $km^3\ yr^{-1}$, constituting a transgression of the PB-W. In contrast to BW, GW encapsulates soil water related processes, flows and stocks (as will be further expounded in chapter 2.3). Although this may be true, Gerten et al. (2015) rebut that BW is regarded as a proxy depicting both BW- and GW-related processes since changes in GW lead to changes in BW and vice versa. Accordingly, calculating them separately distorts and yields overestimations for the current value of the PB-W CV.

Recently, the PB-W's status and its suitability to address hydrological questions at all has been queried by Heistermann (2017) as well as within the subsequent Hydrology and Earth System Sciences journal interactive discussion of the according article (https://www.hydrol-earth-syst-sci.net/21/3455/2017/hess-21-3455-2017-discussion.html, last accessed 13 January 2019). Again, the lacking representation of the green aspect of the water cycle and the upper limit of human perturbations of it within the PB-W is seen as a major weakness of the boundary. This shortcoming of the current definition has been criticized by H.Savenije (RC2 in the interactive comment linked above) and reassured within the reply by M.Heistermann (AC5).

2.3 Green water - the birth of a terminology

First mentioned and defined in the context of water scarcity and quantifications potentials of increases in agricultural production in semi-arid areas by Falkenmark (1995), the concept and terminology of green water has been adopted in many studies and been the subject to diverse definitions (Ringersma et al. 2003; a compilation of definitions can be found in Sood et al. 2014). The manifold yet non-conterminous definitions highlight the difficulty arising from a clear demarcation between GW and BW and what processes to assign to each water fraction (Ringersma et al. 2003; Sood et al. 2014). On the other hand, definitions disagree on whether to include soil moisture, thus liquid GW, or to focus on terrestrial water vapor fluxes alone. In order to further work with the GW-terminology within this study, the definitions given by Schyns et al. (2015) and Sood et al. (2014) will be further specified in the following and is illustrated in figure 2.

2.3.1 Demarcating between blue and green water

The original definition of GW is '*soil water held in the unsaturated zone, formed by precipitation and available to plants*', while BW has been defined as '*liquid water in rivers, lakes, wetlands and aquifers, which can be withdrawn for irrigation and other human uses*' (Falkenmark 1995). Within the scope of this study, green water is defined as a liquid stock of water, consisting of all water in the vadose zone of soils between the wilting point and the maximal water holding capacity (figure 2). The vadose zone is extending from the soil surface to the ground-water, thus BW bearing phreatic zone. A part of this soil moisture might be plant accessible and can thus be made productive for biomass production. Being the balance of outflow and recharge, the GW stock constantly loses and gains water.
GW recharge is either derived from infiltrating terrestrial precipitation or capillary rise from the BW-bearing phreatic zone underneath. When precipitation hits the soil surface, the water is partitioned into infiltration (GW) or surface runoff (BW). The water partitioning depends on (i) the intensity of the precipitation, bearing the potential to exceed infiltration rates, (ii) the soil wetness and infiltration capacity of the upper soil layer, (iii) vegetation and litter cover as well as sealing and crusting and (iv) topographical conditions, such as the position in the slope (Ringersma et al. 2003).

The outflow of GW, in turn, can take place in two directions:
First, solar energy is being consumed to evaporate GW, thus returning a fraction of GW back to generate atmospheric moisture. According to Jung et al. (2010), GW evaporation accounts for half of the solar energy being absorbed by terrestrial surfaces. This terrestrial water vapor flux consists of three different pathways and will hereby be defined as green water flow (GW-flow). Transpiration embodies plant accessible water taken up in the rootzone to balance water losses through the stomata during the CO_2 uptake associated with photosynthesis, by crops and terrestrial ecosystems and is defined as productive GW-flow (Falkenmark and Rockström 2006; Schyns et al. 2015). Unproductive GW-flow, on the contrary, describes GW returned to the atmosphere without being made productive by the biosphere and comprises soil evaporation and evaporation of intercepted precipitation in the canopy.
Second, GW can percolate through the vadose zone by gravitational force, either leading to groundwater formation in the phreatic zone or interflow runoff and subsequent BW formation. The percolation rate is a function of the soil's hydraulic conductivity (Ringersma et al. 2003)

It can be concluded that the balance of GW-stock is the interplay of soil properties (bulk density, water holding capacity and wilting point), climate (precipitation and atmospheric water demands) and vegetation cover density, root structure and water demands (Schyns et al. 2015)

According to this green perspective on the terrestrial water cycle, BW can be redirected to compensate for GW deficiency in form of irrigation. As has been illustrated in figure 2, irrigated BW will subsequently be partitioned into GW (in case of infiltration) or BW (in case of surface runoff). Note that the current definition of PB-W is based on the amount of BW allowed to withdraw for irrigation (WD in figure 2).

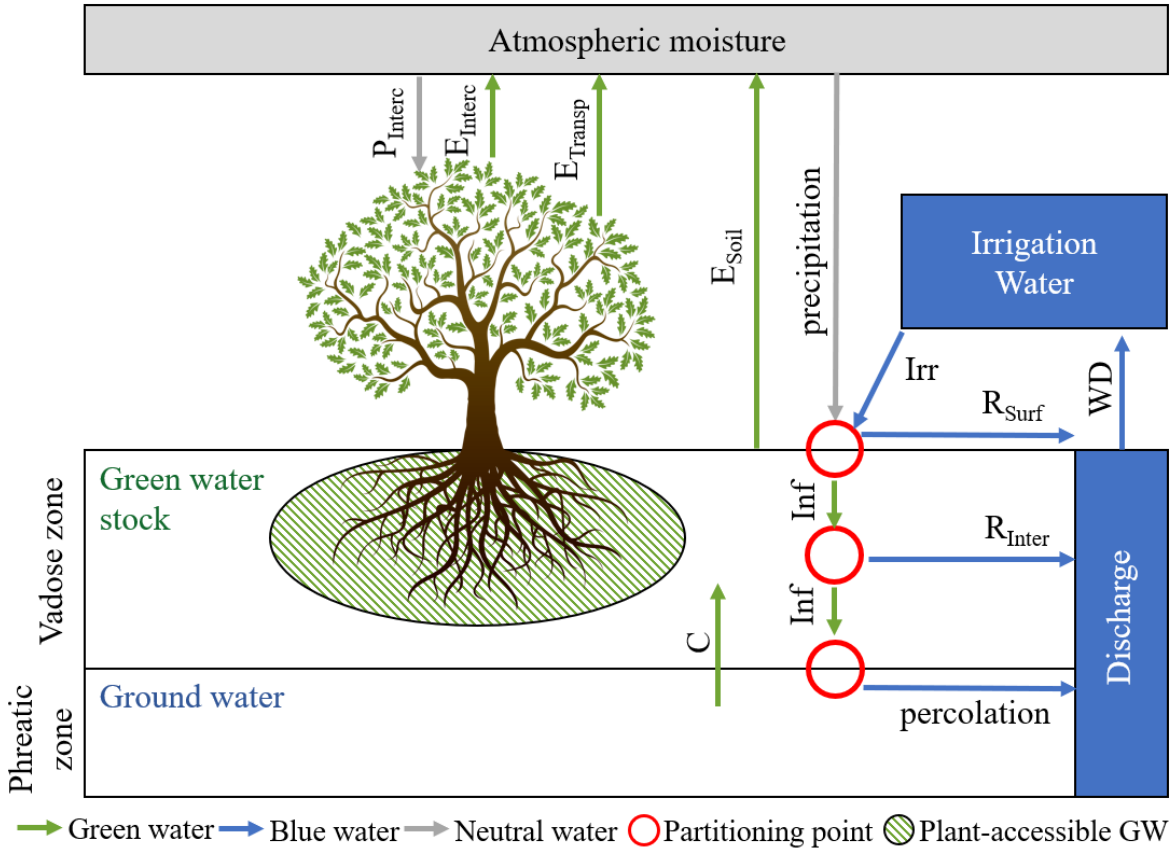

Figure 2. Water color scheme. E_{Interc} – interception, E_{Transp} – transpiration, E_{Soil} – soil evaporation, Inf – infiltration, C – capillary rise, P_{Interc} – intercepted precipitation, R_{Surf} – surface runoff, R_{Inter} – interflow runoff, Irr – irrigation, WD – water withdrawal. E_{Interc} and E_{Soil} together form unproductive GW-flow, E_{Transp} equals productive GW-flow. Water partitioning points are theoretical places of water demarcation. Only a fraction of GW is plant accessible and can be made productive via E_{Transp}. The tree has been adapted from https://ru.kisspng.com/kisspng-kfgk47/preview.html.

2.3.2 Green water availability, deficiency and scarcity

Although water is a renewable resource, both fractions, BW and GW are spatially and temporarily explicitly distributed. This distribution can be expressed in terms of water availability, deficiency and scarcity. Although these concepts are predominantly applied within the BW domain (Vörösmarty et al. 2000; Hoekstra et al. 2012), they can also be used to account for GW. Definitions for the terms are given in table 1. An exhaustive list of GW availability and scarcity indicators has been compiled by Schyns et al. (2015). However, suitable GW indicators for the task at hand, encompassing plant accessible GW availability and GW deficiency, will be introduced in chapter 3.3.

Table 2. Overview of green and blue water related terms and their definitions

Term	*Definition*
Blue water	Liquid stock of water being stored in surface or interflow runoff, water discharge or refreshable groundwater resources
Green water	Liquid stock of water being temporarily stored in the unsaturated vadose zone in soils
Green water flow	Terrestrial water vapor flux, comprising productive (plant transpiration) and unproductive green water flow (evaporation of soil and intercepted water)
Green water availability*	Accessible amount of green water in the plants rootzone in a certain area at a certain time
Green water deficiency	Relation of vegetative green water demand to green water availability.
Green water scarcity	Experienced by a community in a given geographical area over a certain time period during which human green water demand exceeds green water availability

*note that the term GW availability is not per se limited to plant-accessible GW, however, it will be narrowed down to this fraction in the context of this study.

2.4 Green water in the Earth System

2.4.1 The role of green water for biophysical processes

Plant accessible green water, that is plant available water stored in the rootzone, can be made productive and transpired. Vascular plants, in that sense, constitute cohesion-tension driven hydrologic conduits moving water from the soil to the ambient atmosphere by transpiring acquired GW to balance out the water loss experienced during CO_2 uptake (Tyree 1997). The stomata canopy conductance is determining the relationship between GW demand, photosynthesis and subsequently biomass production, and thereby limiting the ecosystem transpiration. However, canopy conductance varies for different vegetation types, heights and stand ages and is tightly linked to the leaf area (Novick et al. 2009). In case of green water stress, GW supply is falling below a certain species-specific threshold of GW demand (GW deficiency), causing the actual canopy conductance to fall behind the potential canopy conductance (Gerten et al. 2007) and leads eventually to wilting (Smith and Griffiths 1993). Accordingly, GW deficiency is co-limiting transpiration and photosynthesis and thereby carbon assimilation and biomass production and follows a growth seasonal pattern (Gerten et al. 2007). In a recent study, Humphrey et al. (2018) were able to clarify the link between atmospheric CO_2 growth rates and GW deficiency by studying terrestrial water storages with the help of satellite gravimetry observations. Drier years, they conclude, lead to lower carbon fixation potentials due to the experienced water stress.

It can be concluded that the experience of water stress is directly linked to the replenishment of GW which, in turn, is again linked to precipitation and the subsequent water partitioning into BW and GW (cf. figure 2). In the following, the concepts of moisture recycling and precipitationsheds will be introduced to reveal how atmospheric moisture and thus precipitation is related to GW.

2.4.2 Moisture recycling and precipitationsheds

By utilizing an accounting model to trace back the origin of atmospheric moisture, van der Ent et al. (2010) found that large portions of terrestrial precipitation are sustained by terrestrial evapotranspiration, thus GW-flow. They found that 40% of global terrestrial precipitation have previously been evapotranspired (GW-flow) and 57% of all GW-flow is subsequently precipitating over land again. Globally, recycled GW-flow has been estimated to mount up to 31,600 – 42,000 $km^3\ yr^{-1}$ (Falkenmark et al. 2019). The interdependency of precipitation and GW-flow is known as moisture recycling or the moisture feedback, stating that land surfaces receive GW-flow-derived precipitation. Correspondingly, the cycling of moisture between land and atmosphere can either be accelerated or decelerated by faster or slower GW-flow rates. Moisture recycling operates on both regional and continental levels. While regional moisture recycling refers to precipitation of atmospheric moisture mainly stemming from GW-flow from the same region, continental moisture recycling, in turn, encompasses precipitating moisture originating from a different source area and is thus more susceptible to atmospheric moisture transport mechanisms. On a global scale, regional moisture turnover rates are highest in the Amazon and Congo basins as well as in the Tibetan plateau, while most moisture recycled on a continental scale stems primarily from the entire Amazon basin, Eastern Africa and large parts of central Asia (van der Ent et al. 2010).

Like a watershed, where upstream and downstream of a river are connected by runoff, a precipitationshed constitutes an approach to connect the atmospheric river of upwind ocean or terrestrial evaporation from the moisture source area with downwind precipitation in the sink area (figure 3). According to Keys et al. (2012), a precipitationshed is being defined as the probabilistic source area where 70% of the evaporation sustaining the precipitation in a sink area originate from. The core precipitationshed is contributing a vital amount of moisture stemming from GW-flow to the sink region. Interannual variabilities in core precipitationsheds could be traced back to fluctuations in GW-flow (Keys et al. 2014). This claim is supported by a remote sensing study of the tropics conducted by Spracklen et al. (2012), showing that more atmospheric humidity was maintained when air passed over areas areas with denser vegetation, providing extensive GW-flow, as compared against areas with sparse vegetation. Upwind land-use in the terrestrial source area of a precipitationshed has therefore a direct impact on the amount and regularity of downwind precipitation. The concept has been further developed by Weng et al. (2018), introducing ‘most influential precipitationsheds’ (MIPs) to highlight the most influential source areas for GW-flow. Precipitation in the source area are therefore most sensitive to (anthropogenic) shifts in GW-flow amount and composition within MIPs.

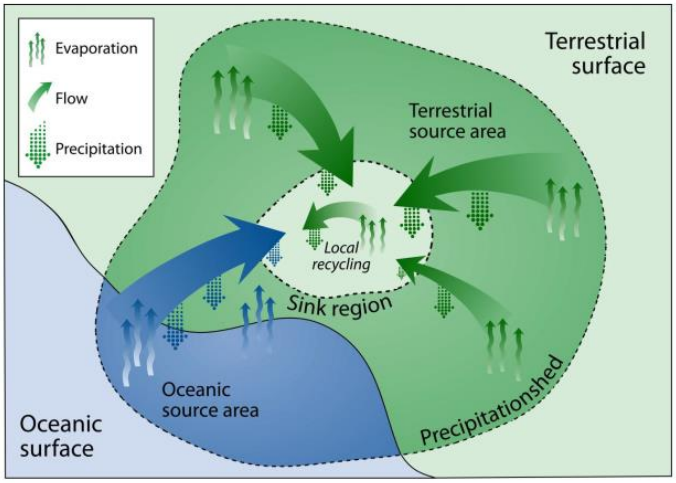

Figure 3. Precipitationshed draft; reprinted from Keys et al. (2012), shared under the Creative Commons Attribution 3.0 License.

In summary, these 'invisible' atmospheric rivers providing humidity for precipitation in the sink area are susceptible to alterations in the replenishment of GW and subsequent amplified or reduced GW-flow in the terrestrial source area, first and foremost within MIPs. It has been shown that moisture recycling within precipitationsheds is not only playing a vital role in providing sufficient water for vulnerable and rainfed agriculture dependent human societies (Keys et al. 2012), but are also vital in providing and maintaining ecosystems and thereby ecosystem services (Keys et al. 2016). The Janus-faced impact of ALC on GW-flow will further be elaborated in chapter 2.4.

2.4.3 Green water – climate interaction

Taking water related atmospheric processes and feedbacks into account is far beyond the scope of this study, nonetheless its worth mentioning that GW plays a vital role in climate and vice versa. To illustrate, 50% of the incoming solar radiations energy be absorbed by land surfaces is consumed to evaporate GW, causing a surface cooling (Jung et al. 2010). Atmospheric moisture, in turn, is a key uncertainty in future climate projections (Held and Soden 2000). Once being in the atmosphere, water is a strong greenhouse gas and leads to changes in the adiabatic lapse rate. This very brief introduction underlines the necessity for future studies to determine green waters' impact on the climate system within the PB framework. The impact of future climate change on GW, on the other hand, must be studied closely as well, as fossil records point towards an accelerated water cycle in periods of higher atmospheric temperatures (Bowen 2011).

2.4.4 Green water related tipping points in the earth subsystems

Various ecosystems can have at least two alternative stable states of existence. Regime or state shifts can occur when an environmental control parameter changes, favoring the emergence of the previously suppressed alternative stable state (Scheffer et al. 2001; Scheffer et al. 2009). Such a shift can either occur in a smooth and slow transition or in an abrupt and non-linear fashion. An abrupt change encompasses reaching a crucial threshold, a so-called tipping point (Lenton et al. 2008). Large-scale components (such as a collection of regions) of the ES, bearing an intrinsic tipping point, are referred to as tipping elements. Evidence exists that planetary-scale shifts in the biosphere have occurred in the Earth's past, for example the shift between the two stable states of atmospheric oxygen concentration during the 'Great Oxidation' event, 2.4 billion years ago and the subsequent ecological reaction to it (Barnosky et al. 2012; Lenton and Williams 2013). Tipping elements do, however, not necessarily need to affect the earth system as a whole but are often more tightly linked to regional subsystems. Nevertheless, the understanding of how anthropogenic GW perturbations can force large regime shifts or approximate tipping points is still limited. Table 2 shows the potential GW-related tipping points or non-linear shifts identified so far.

Table 3. Green water related tipping elements.

Tipping element	*Control parameter**	*Regime shift*	*Incidence*
Amazon rainforest	GW-flow [a,b,c]	Forest dieback	8–3.6 kyr BP [d]
Indian summer monsoon	GW-flow [f]	Monsoon weakening	8.2 kyr BP [g]
West African monsoon	GW-flow [a,e]	Sahara greening	15–5 kyr BP [e]

*Only GW-related control parameters are listed in the table

[a] Lenton et al. (2008)

[b] Zemp et al. (2017)

[c] Hirota et al. (2011)

[d] Mayle et al. (2004)

[e] Gaetani et al. (2017)

[f] Pathak et al. (2014)

[g] Dixit et al. (2014)

Amazon rainforest:

It has been estimated that 25-50% of precipitating moisture in the Amazon rainforest are regionally recycled (Eltahir and Bras 1994; van der Ent et al. 2010), thereby making the ecosystem vulnerable towards a reduction of GW-flow. Weng et al. (2018) successfully demonstrated that atmospheric moisture supply is especially vulnerable towards deforestation-induced interruptions of the vegetation-atmosphere moisture feedback within MIPs. A combination of climate change, deforestation and wildfires could potentially trigger a self-amplified, non-linear tipping point in the Amazon basin, coined as the Amazon forest dieback (Nepstad et al. 2008; Zemp et al. 2017), causing the alternative stable state of a savannah-like ecosystem to establish (Staver et al. 2011; Hirota et al. 2011). Spracklen et al. (2012) estimated that unimpeded deforestation at the current speed would cause a decrease in precipitation by 12% and 21% in wet- and dry-season respectively by the year 2050. Evidence exists that a partial drying and regime shift within the Amazon occurred in Earth's past. Fossil pollen

records indicate that the reduced precipitation of ca 40% during the Mid-Holocene (8,000–3,600 BP) led to a succession of savannah taxa in parts of Amazonia (Mayle et al. 2004).

Indian summer monsoon:
Driven by a land-to-ocean pressure gradient, the monsoon circulation is highly susceptible towards any changes among the temperature and moisture gradients. Lenton et al. (2008) argue that while the monsoon might benefit from an amplified temperature gradient under climate change, a decrease in Albedo tend to weaken the wet Indian summer monsoon, pushing it towards a stable state with low precipitation (Zickfeld et al. 2005). A weakening of the monsoon could lead to widespread aridification with catastrophic effects on ecosystem and human societies. Although most of the moisture sustaining the monsoon stems from oceanic sources, terrestrial moisture recycling plays a crucial role for the Indian summer monsoon and can account for up to 25% of the precipitation at the end of monsoon (Pathak et al. 2014). Changes in GW-flow causing a deceleration of the moisture feedback can therefore weaken the monsoon circulation. Paleoclimatic records provide evidence for several intervals of a deteriorated Indian summer monsoon during the Holocene (Gupta et al. 2003) and an abrupt desiccation at 8.2 kyr BP (Dixit et al. 2014).

West African monsoon:
Precipitation in West Africa is concentrated in the summer months of the northern hemisphere and relies on the West African monsoon. Observable changes in the monsoon regime and strength are linked to multiple factors and reliable predictions are still a major uncertainty in climate modelling (Gaetani et al. 2017). Increased summer precipitation during the so-called African Humid Period (15-6 kyr BP) increased GW availability and led to an extension of grass- and shrubland far north, causing a greening of the Sahara (Patricola and Cook 2007). Extensive ALC in the area degrades vegetation, casuing a reduction in GW-flow and subsequently in atmospheric moisture with adverse consequences on moisture recycling (Boone et al. 2016). Lenton et al. (2008) on the other hand, argue that higher sea surface temperatures resulting from climate change in the 21st century can increase the inflow of moisture, potentially shifting precipitation regimes towards a subsequent greening of the Sahara. The role of human perturbations of the ES on this tipping point are therefore ambigious.

The tipping points in subsystems of the ES mentioned above are primarily prompted by changes in sea surface temperature, aerosol loading or surface albedo. Nonetheless, they are also at least partly related to precipitation variability and reduction and thus to local or precipitationshed-scale moisture recycling. Anthropogenic changes in GW-flow and thus in moisture recycling are multifaceted and can either catalyze (Indian summer monsoon), dampen (West African monsoon) or force (Amazon rainforest) reaching tipping points.

2.5 Anthropogenic changes in green water

How humankind has been altering precipitation by land-use and water management has been subject to debates since the late 19th century and ranged from positive attributions to atmospheric moisture from land cultivation, e.g. the legend that “the rain follows the plough”

(Dirmeyer and Brubaker 2007; and references therein), to integrated moisture budget models and formulas which provide a far more differentiated image (van der Ent et al. 2010; and references therein). Green water plays a variety of roles and functions for humanity and is subject to manifold human perturbations on different scales (Falkenmark et al. 2019). In general, human perturbations of the terrestrial water vapor flux (GW-flow) and consequently precipitation can be aligned along two axes. Modifications, leading to an amplified GW-flow, thus contributing to a faster moisture recycling on the one hand and modifications entailing a reduction of GW-flow, thus contributing to a slower moisture recycling, on the other hand.

Land cover modifications leading to an amplified GW-flow:
Irrigation, that is redirected runoff (BW) to compensate for GW deficiency in agricultural production, contributes to additional atmospheric moisture since irrigation water forms GW which can eventually evaporate. The effectiveness of the irrigation strategy, in terms of biomass production, is determined by how much of the irrigated water takes the productive GW-flow pathway and how much is either lost by unproductive evaporation or by BW formation at the two water portioning points. However, regardless of the GW-flow pathway, more GW-flow is contributing to atmospheric moisture and thus downwind precipitation. To illustrate, land cover changes in Colorado from steppe to cropland increased GW-flow by 120% in case of irrigated crops (compared against 3% for non-irrigated crops), since more GW was available for GW-flow (Baron et al. 1998). On a global scale, it has been estimated that GW-flow amplification due to irrigation accounts for 2600 $km^3\ yr^{-1}$ (Gordon et al. 2005) and accordingly contributing positively to the moisture recycling feedback (figure 4b).

Land cover modifications leading to a reduced GW-flow:
Changing land-use by deforestation, overgrazing or surface sealing will reduce GW-flow (van der Ent et al. 2010). Water partitioning into GW and BW at the land surface is easily disturbed by deforestation and grazing, favoring higher runoff rates (BW) at the expense of infiltration, thus GW formation (Zhang et al. 2014). In addition, the decreased rooting depth of the anthropogenic replacement of the forest can only take up GW at shallower soil layers, leading to higher drainage at the second water partitioning point within the soil, thereby favoring groundwater formation (BW) at the expense of the GW stock. A synthesis of 94 catchment experiments compiled by Bosch and Hewlett (1982) came to the conclusion that there is a strong positive relationship between clear-cut and runoff yield by the watershed. This conclusion is underpinned by the estimation that ALC led to an increased runoff by 7.6% if compared against potential natural vegetation (PNV) on a global level, mainly stemming from deforestation, urbanization and grazing (Sterling et al. 2012). The subsequently reduced GW-flow has a negative impact on atmospheric moisture which, in turn, leads to a decelerated moisture recycling feedback (figure 4a). The reduced moisture turnover rate, in turn, is negatively affecting terrestrial ecosystems and rainfed agriculture downwind. To illustrate, vast expansions of crop- and grasslands to the expense of forests in Australia over the course of the last 200 years led to a decrease in GW-flow by approximately 10%, eventually leading to reduced crop productivity (Gordon et al. 2003).

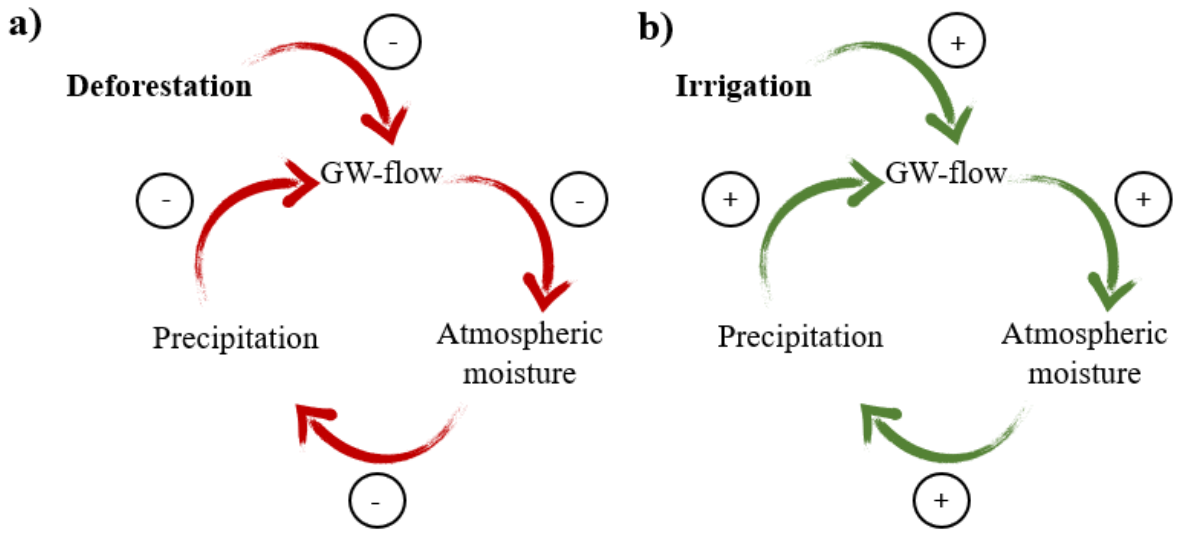

Figure 4. Positive and negative impacts of human activity on the moisture recycling feedback. In general, reducing or redirecting runoff results in an increase of GW-flow, while every increase of runoff leads to a GW-flow reduction, with positive, respective negative effects on moisture recycling.

On a global scale, the net changes in GW-flow (amplifying and mitigating) are nearly balancing each other. A modelling study conducted by Gordon et al. (2005) concluded that deforestation accounted for a reduction in GW-flow in the order of 3,000 $km^3\ yr^{-1}$, or about 4% of the total GW-flow. This loss of water vapor flow is almost entirely offset by the amplified GW-flow due to irrigation, summing up to about 2,600 $km^3\ yr^{-1}$. However, these numbers do not reflect decisive spatial heterogeneities of anthropogenic GW-flow perturbations and their impact on natural ecosystems and rainfed agriculture and thus the functioning of the ES. In addition, GW-flow changes highly depend on the natural status of a given ecosystem, thus its potential natural vegetation (PNV), which is subsequently put under ALC. A conversion from wetland to non-irrigated cropland reduces GW-flow by 106%, whereas transforming barren land to irrigated cropland amplifies GW-flow by 200%, on average (Sterling et al. 2012).

Human perturbations are not limited to the overall GW-flow but also affect the proportion of individual GW-flow components. While a reduction in interception loss and transpiration after clear-cutting were observed in the field (Swift Jr. et al. 1975), comprehensive studies about land use effects on GW-flow composition are very limited, as has been pointed out by Rost et al. (2008b).

In order to maintain a well-functioning state of the ES, it is thus important to address human-driven global change of GW to manage and prevent GW-related tipping points. However, the water image of management institutions and policy makers is dominated by BW, while GW is still playing, at most, a subordinate role (Vörösmarty et al. 2000; Rockström et al. 2009a; Sood et al. 2014).

3. Methods

3.1 The LPJmL Model

3.1.1 Model description and justification

In general, modelling global GW-stocks and GW-flows can either be undertaken from an atmospheric or landscape perspective. Jaramillo and Destouni (2014) found out that the landscape drivers, such as anthropogenic land use, mostly outweigh climatic drivers for the observable changes in GW-flow, which therefore justifies a landscape-based model selection.

To simulate the impact of anthropogenic perturbation on GW from a landscape perspective, the fourth version of the process-based global dynamic vegetation and water balance model 'Lund-Potsdam-Jena with managed Land' (LPJmL) has been employed (Schaphoff et al. 2018). LPJmL computes large-scale terrestrial ecosystem processes in a spatially (0.5° x 0.5° grid cells) and temporally (up to daily) explicit framework. Being based on LPJ (Sitch et al. 2003), LPJmL has been further developed to account for different scenarios and water fluxes as a response to changed climatic forcing or human land management. Since its release in 2007, LPJmL has being used in nearly 100 published scientific studies covering a variety of topics (the full list can be found in the supplementary information of Schaphoff et al. 2018). Moreover, the model has been extensively validated against observational data for a large variety of biogeochemical and hydrological parameters, such as runoff and evapotranspiration (Gerten et al. 2004) or soil moisture (Wagner et al. 2003). Additional model validation is given in Bondeau et al. (2007).

For the task at hand, LPJmL is found to be highly suitable. First, the model can distinguish between 11 Plant Functional Types (PFT) as well as 16 Crop Functional Types (CFT) which can either be rainfed or irrigated. This variety allows LPJmL to simulate the most important biomes and anthromes and therefore PNV and ALC (Appendix A). Different PFTs and CFTs can co-inhabit a grid cell and each of the plant and crop functional types is characterized by specific physiological, phenological, morphological and bioclimatic traits (a full list can be found under: https://github.com/PIK-LPJmL/LPJmL/blob/master/par/pft.par, last accessed 13 January 2019), allowing for a realistic representation of the linkage between vegetation and the water cycle. In addition, LPJmL4 is capable of dynamic vegetation processes. This incorporates sapling establishment, background mortality and stress mortality for PFTs (Schaphoff et al. 2018). The dynamic representation of natural and managed ecosystems makes LPJmL highly suitable to account for changes in the water cycle stemming from the PNV to ALC conversion.

3.1.2 Terrestrial water balance in LPJmL

In principle, all water-related processes necessary to demarcate between BW and GW based on the definition given in chapter 2.3.1 are simulable within LPJmL4. An exhaustive overview of the calculations and influencing parameters can be found under Schaphoff et al. (2018). However, processes vital to interpret the output are briefly stated below.

The assumption is made that soils are composed of five horizontal layers whose hydrological characteristics are based on soil textures derived from the Harmonized World Soil Database for each grid cell (Nachtergaele et al. 2009). Of paramount importance are the water holding capacity and wilting point, defining the infiltration rate and plant available soil water, respectively. Precipitated or irrigated water is infiltrating unless the water saturation of the soil is exceeded. Surplus surface water is subsequently creating surface runoff and can thus be regarded as BW. In addition to surface water, runoff is created by latent water movement between the cells. By gravitational force, soil water can percolate through the profile to create groundwater, partitioning between BW and GW. Soil water content is thus a temporal storage defining the potential of terrestrial water vapor fluxes to match atmospheric water demands. Incoming solar radiation is vaporizing terrestrial water either by evaporating intercepted precipitation in the canopy (interception loss), evaporating soil water from the upper layer of bare soils (soil evaporation), or the coupled carbon uptake and transpiration flow by plants defined by the stomata conductance (transpiration). Note that soil evaporation occurs only from unvegetated areas within a given grid cell.
In addition, LPJmL4 allows to account for irrigation, that is redirected BW, in case the CFT water demand is higher than the GW availability to maintain transpiration. Infiltration of redirected BW thus leads to GW formation. The most important irrigation systems (surface, sprinkler and drip irrigation) are featured (Schaphoff et al. 2018). In LPJmL4, irrigation water is taken from the river discharge, not surface runoff.

3.2 Simulation protocol

While the establishment of PFTs is determined by their bioclimatic constraints during the model spin-up and preindustrial period, the cultivation of crops, and thus their spatial distribution, is defined by a land-use input file.

Data bases:
The historical land use and climate data files employed to prescribe the fractional coverage and distribution of CFTs and to force the model were taken from the updated Inter-Sectoral Impact Model Intercomparison Project (ISI-MIP2b). ISI-MIP2b is a consistent cross-sectoral dataset synthesizing multi-model climate impact projections on agriculture, water and biomes (Frieler et al. 2017; publicly available under: https://www.isimip.org/protocol/#isimip2b, last accessed 13 January 2019). Since no climate change scenarios are being considered under the research objective of this study, only the historical land use and climate data sets of ISI-MIP2b, covering the 145 year period between 1861-2005 have been employed.

Model run set-ups:

Starting at zero, all water and carbon pools as well as all PFTs are establishing and reaching a state of equilibrium over the course of the 5,000-year-lasting spin-up period (piControl protocol). The climatic conditions during the spin-up period are oscilating within the preindustrial climatic variance. Next, during the preindustrial phase of the simulation protocol, land-use as being prescibed by the input data file, is introduced. The last 145 years of the simulation period from 1860 onward, constitute the industrial phase charaterized by an increase in greenhouse gas concentrations (figure 5). Note that the output data was only created for this period (1860-2005).

Three different simulation scenarios were conducted to calculate hydrological parameters under a potential 'natural state' with PNV, as well as under a 'actual state' with ALC with and without irrigation (table 3):

Table 4. Simulation run set-ups and descriptions

RunID	*Description*	*Vegetation*
PNVr	'Natural state', no human interaction, full potential natural vegetation coverage	PFT
ALCr	anthropogenic land cover without irrigation	PFT, rainfed CFT
ALCr_irr	'Actual state' anthropogenic land cover with irrigation	PFT, rainfed CFT, irrigated CFT

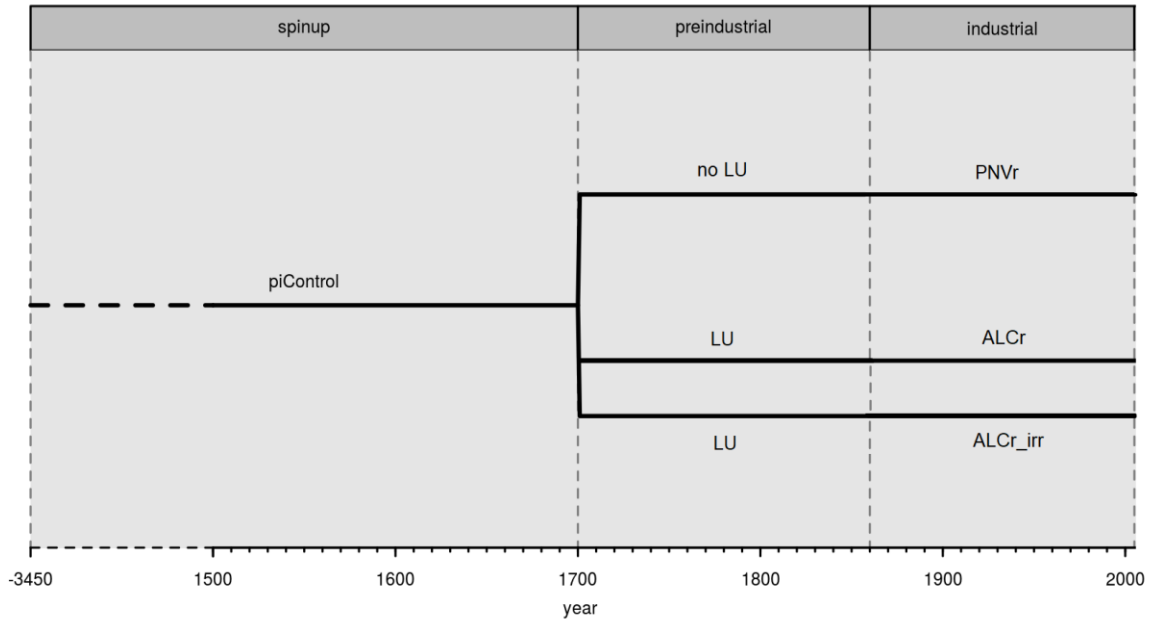

Figure 5. Simulation protocol of the three different scenarios as performed in LPJmL4. LU – land-use. PNVr – potential natural vegetation simulation run, ALCr – anthropogenic land cover simulation run, ALCr_irr – anthropogenic land cover simulation run with irrigation schemes. All model runs were conducted with the same spin-up protocol and climate forcing but differ in terms of land-use (LU).

3.3 Measuring green water

GW availability (GW_{avail}):
Following the GW indicator classification given by Schyns et al. (2015), absolute GW is classified as all plant available GW, regardless of the actual vegetation GW demand. The amount of available GW at a specific place and time is, as has been pointed out above, the balance of GW outflow and recharge and thus the equilibrium of infiltration, percolation, soil evaporation and transpiration. LJPmL4 provides the output 'rootmoisture', classified as all plant accessible soil moisture between the wilting and saturation point. The accessibility of soil moisture for plants depends on the PFT/CFT-specific root distribution in each of the five soil layers. The higher the root density in a soil layer for a given vegetation type, the more of the soil moisture in the layer is plant accessible. Same applies for the rooting depth. 'Rootmoisture' matches the definition of plant accessible GW in chapter 2.3.1. By implication, root moisture is dependent on, but not congruent with soil moisture.

GW-flow efficiency (GW_{eff}):
The GW-flow efficiency indicator (GW_{eff}) has been conceptualized within this study, borrowing from Rockström et al. (2007) who previously defined an index for GW productivity under agricultural production. GW_{eff} is defined as the ratio of productive to unproductive GW-flow while considering GW-flow for a given cell in relation to the global maximum GW-flow value. The computation of the indicator is broken down into single-steps below:

$$(1)\ \text{GW-flow} = E_{Transp} + E_{Soil} + E_{Interc}$$

The total GW-flow for a given cell is the sum of its individual productive and unproductive GW-flow values, with E_{Transp} being transpiration, E_{Soil} soil evaporation and E_{Interc} evaporation of intercepted water.

$$(2)\ g = \frac{\text{GW-flow}}{\text{GW-flow}_{max}}$$

Next, the cell-specific weighting factor g will be calculated as the ratio between the cells GW-flow value and the maximal GW-flow value of the three conducted simulation runs (GW-flow_{max}). Thus, g ranges between zero and one, with one representing grid cells with highest simulated GW-flow values.

$$(3)\ GW_{eff} = \frac{E_{Transp}}{\text{GW-flow} * g}$$

Subsequently, GW_{eff} will be calculated as the ratio between productive and overall GW-flow while considering the weighting factor g.

The indicator has been compiled to depict how much of the terrestrial water vapor flux is made productive by the biosphere and how much is lost unproductively. Differences in this indicator for different simulation runs will show to what extent this GW usage efficiency has been

shifted. However, the GW_{eff} indicator is only capable of surfacing a shift between the ratio of productive to unproductive GW-flow but is not suitable to indicate green water related stress of the biosphere. To fill this gap, the more mature indicator L_{TA}, dedicated to monitor the canopy water conductance, will be introduced below.

GW deficiency (L_{TA}):
The effectiveness of water conductance through the canopy is generally determined by the stomatal conductance (Novick et al. 2009). However, the actual canopy conductance can fall below the potential canopy conductance in case root moisture, thus available GW, is lower than the vegetation water demand at a given space and time. Gerten et al. (2007) propose a biome-level water limitation index (L_{TA}), accounting for the ratio between potential and actual canopy conductance. L_{TA} indicates if the actual productive GW-flow falls behind the potential productive GW-flow due to GW-related stress. In other words, if productive GW-flow and thus photosynthesis are co-limited by GW deficiency. In case the index is at one, no water stress has been experienced for the time period being measured, however, if the index drops towards zero, higher rates of water limitation are experienced.

3.4 Data processing and visualization

All but the L_{TA}-index output data are comprised of monthly values for the simulation period of 145 years (1861 – 2005) for the 67420 terrestrial 0.5° x 0.5° grid cells.
The GW limitation index L_{TA}, in turn, is biome specific and accounts for 11 PFTs, 16 rainfed CFTs and 16 irrigated CFTs (cf. Appendix A for a full list), thus 43 individual bands. The L_{TA} output data is comprised of yearly values for the 145 years lasting simulation period for 43 bands in a spatial resolution of 67420 terrestrial 0.5° x 0.5° grid cells.
Grid cell average outputs over all PFTs and CFTs do not allow biome-specific assertions of GW related parameters (such as transpiration, interception or runoff)

In general, no extensive data processing was applied. Monthly average values for the last 30 years of the simulation period (1976-2005) were calculated to minimize inter-annual and intra-annual variations (Arguez and Vose 2011). In addition, the L_{TA} output was subsequently weighted by the coverage of each band in the specific grid cell to gain a grid-cell-based average value.

In order to depict changes of the ALC conversion, the grid cell values of various GW-related parameters for ALCr and ALCr_irr, respectively, were subtracted from PNVr. In addition, to gain a global average of the gains and losses of each GW parameter, difference values were multiplied by their specific grid cell area to account for the spatial dimension and the Earths spherical shape, multiplied by 12 to gain an annual value and subsequently divided by 10^{12} to obtain values in km^3 per year.

For the creation of maps, the grid cells for both the output values as well as the difference values needed to be rasterized, considering their longitudinal and latitudinal values. Next, the Robinson projection, as a good compromise between equal-area and conformal projections,

and continuous color ramps have been chosen. Continuous color ramps have the advantage to visualize data as a continuum without the need for classification. Note that even though the same color ramp palettes have been used for all mapped parameters, the limits of the ramps vary as well as their biases for color spacing. Lastly, regional intra-annual trendlines were created.

4. Results

4.1 Globally aggregated values

In general, ALC conversion led to changes among all GW-related parameters (table 4). Although total GW-flow, thus transpiration, soil evaporation and inception loss together has only been neglectable decreased from 70,150 $km^3\ yr^{-1}$ under PNVr to 69,946 $km^3\ yr^{-1}$ under ALCr_irr, big shifts were simulated for the individual components of GW-flow. Global transpiration values dropped by 1.13% from 53,254 $km^3\ yr^{-1}$ (PNVr) 52,651 $km^3\ yr^{-1}$ (ALCr_irr), a contrary trend can be seen for soil evaporation. It has been simulated that soil evaporation increased by 5.75% from 8,874 $km^3\ yr^{-1}$ to 9,384 $km^3\ yr^{-1}$. Evaporation of interception water, on the other hand, decreased by -1.38%, indicating a decline in leaf surface area intercepting precipitation. Surprisingly, a minor positive change can be seen regarding GW availability. On the contrary, runoff generally increased, thereby implying that less water was able to infiltrate, benefiting BW formation. Percolation was not quantified but the output discharge (Appendix E) is formed as the sum of runoff and percolation. As can be seen in table 4, a mismatch between the results of this study and prior studies can be witnessed. Potential explanations for the disagreement will be given in the discussion (chapter 5.2).

Table 5. Global values of GW related parameters under PNVr and ALCr_irr, the percentual differences between the two runs and reported earlier estimates.

GW parameter	*PNVr ($km^3\ yr^{-1}$)*	*ALCr_irr ($km^3\ yr^{-1}$)*	*Change (in %)*	*Earlier estimates (ALC) ($km^3\ yr^{-1}$)*
GW (root moisture)	25,807	25,927	0.47	N/A
GW-flow	70,150	69,946	-0.003	53,500-72,500 [a,b,c,d,e,f,g]
Transpiration	53,254	52,651	-1.13	37,500 – 38,500 [f,d]
Soil evaporation	8,874	9,384	5.75	18,000 [f]
Interception loss	8,022	7,911	-1.38	6,000 [f]
Runoff	60,654	61,171	0.85	53,500 [g]

[a] Baumgartner and Reichel (1975)
[b] Rockström et al. (1999)
[c] Gordon et al. (2005)
[d] Gerten et al. (2005)
[e] Rost et al. (2008a)
[f] Rost et al. (2008b)
[g] Sterling et al. (2012)

Even though global averages are representative for the overall tendency, they fail to account for subglobal, thus regional, differences. Regional differences are by definition larger than the global sum of all positive and negative changes which are often cancelling each other out (figure 6). Here, largest changes occur for soil evaporation in relative numbers (percentual change) and for soil evaporation and transpiration in absolute numbers (change in $km^3\ yr^{-1}$). Differences between ALCr and ALCr_irr are surprisingly little, but irrigation leads to a smaller increase in discharge, compared with PNVr (+ 0.5% for ALCr vs. + 0.33% for ALCr_irr, cf. Appendix E), since discharge is redirected for field irrigation. By applying BW on agricultural land, more GW is being made available while simultaneously increasing runoff due to irrigation water that cannot infiltrate. The resulting higher GW availability (and overall soil moisture), in turn, leads to increased soil evaporation and transpiration rates, as can be seen in figure 6. Evaporation of interception is nearly unaffected since irrigation water cannot be intercepted, however, a slight increase under ALCr_irr can be seen, presumably since more biomass is growing under irrigation. The differences between ALCr and ALCr_irr and the parameter sum values in general are comparably small on a global scale but can lead to big local differences. Note that the positive and negative changes in figure 6 are not resolving positive or negative changes within a grid cell, but the mean of positive and negative changes within a grid cell.

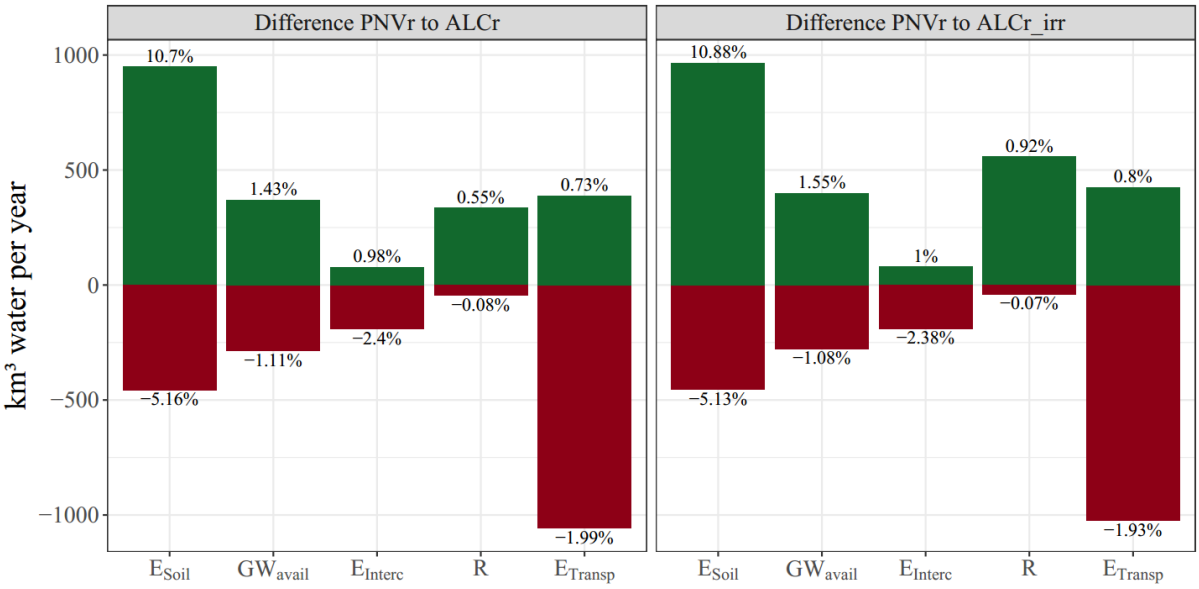

Figure 6. Sum of all positive and negative changes for various GW-related parameters as the difference between the PNVr and ALCr (on the left), and the differences between the PNVr and ALCr_irr (on the right). The sum values are derived by grouping grid cells into positive or negative cell means and subsequently summing them up. E_{soil} – soil evaporation, GW_{avail} – plant-available GW, E_{Interc} – interception, R – runoff, E_{Tranp} – transpiration.

4.2 Global maps

4.2.1 Deforestation and irrigation changes on GW-flow

By decreasing infiltration and increasing runoff, deforestation (as the major impact of ALC conversion) is decreasing GW formation while benefiting BW. This shift eventually leaves less GW for the atmospheric evaporation and transpiration demands, resulting in a reduction in GW-flow. To account for the impact of ALC conversion alone, the sum of transpiration, soil evaporation and interception (total GW-flow) of PNVr have been set off against ALCr (figure 7a). On the flipside, this trend is being counteracted by the redirection of BW due to irrigation schemes (figure 7b). To quantify the redirection and the terrestrial vapor fluxes from redirected BW, the ALCr has been set off against the ALCr_irr. However, combining the findings of figure 7a and 7b highlights the spatial variation of anthropogenic induced GW-flow changes, although deforestation and irrigation are partly offsetting each other on a global level. In general, the changes are well aligned with areas of intense land cover change and irrigation (figure 9).

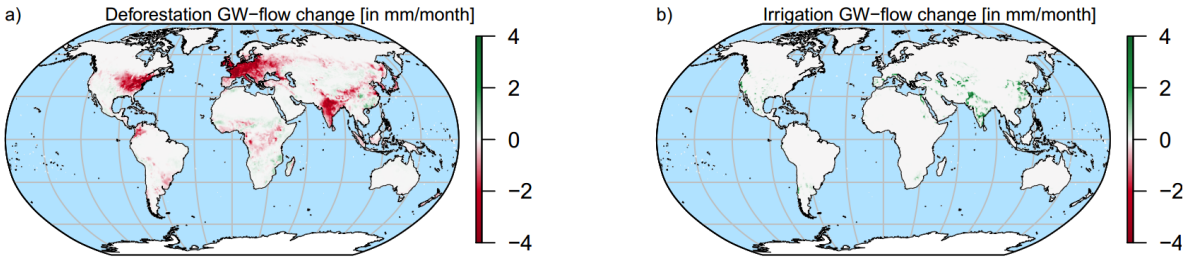

Figure 7. Deforestation and irrigation GW-flow changes; split into the induced changes by a) land cover conversion from PNV to ALC and b) the redirection of BW as irrigation water.

4.2.2 Changes in GW availability, GW_{eff} and L_{TA}

The left column of figure 8 shows global maps of the annual average of GW availability, GW_{eff} and L_{TA} as being simulated for PNVr, while the right column of the figure displays changes caused by human interaction with the ES (that is the difference between PNVr and ALCr_irr).

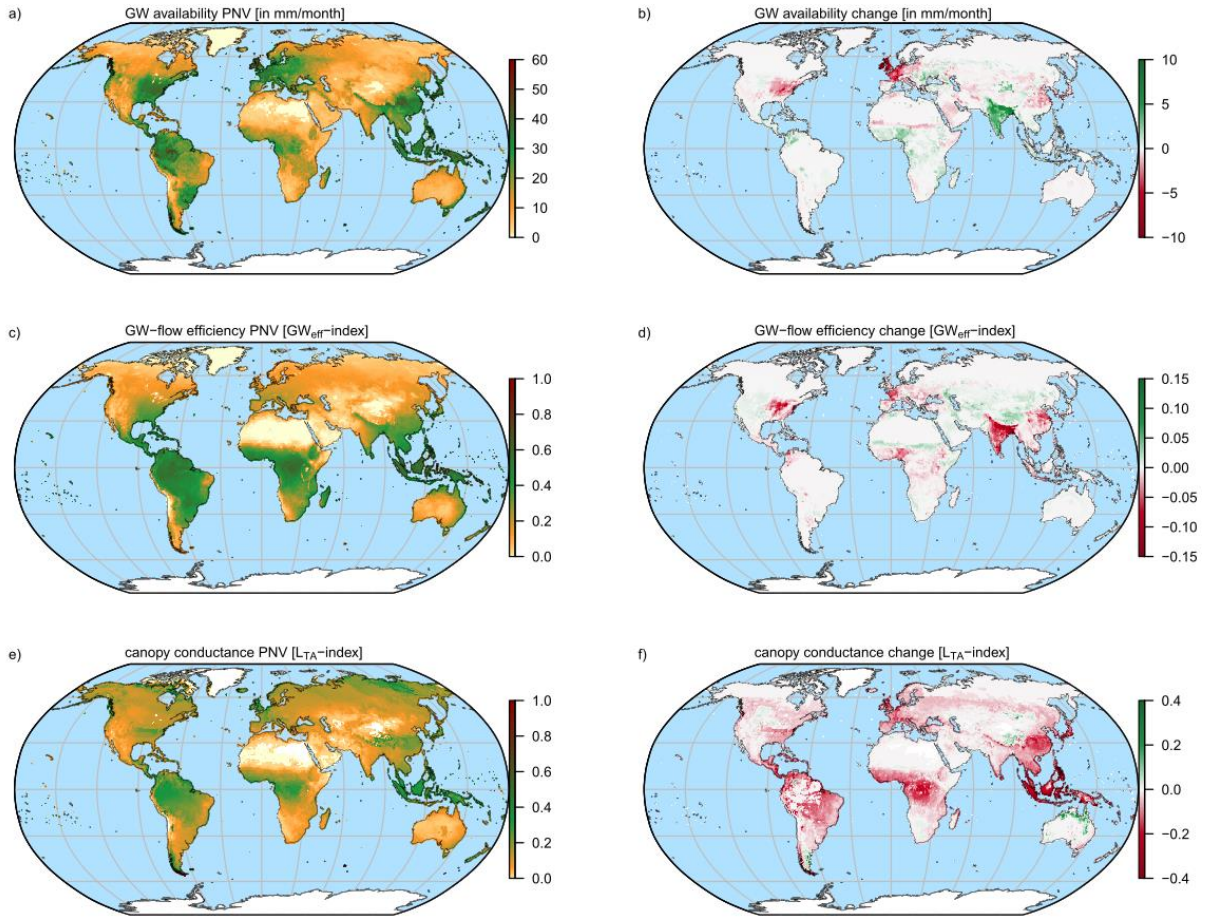

Figure 8. GW availability, GW_{eff} and L_{TA}; results for PNVr are mapped in the left column, while the column on the right depicts the respective human perturbations and are calculated as the difference between the 'natural state' (PNVr) and the 'actual state' (ALCr_irr) simulations.

GW availability (GW_{avail}):

Simulated GW availability under PNVr, thus plant available soil moisture, is varying considerably around the globe as a function of precipitation variations, varying vegetation cover type and density and infiltration rates of precipitation (figure 8a). Low liquid precipitation rates and/or sparse vegetation coverage in deserts and high latitudes result in close to zero GW availability. On the flip side, high precipitation rates lead to high GW availability in the humid and subhumid tropics, particularly in the Amazon basin and Southeast Asia, while deep rooting depths under PNV biomes could be a potential explanation for the large availability of GW in central Europe and parts of North America under a 'natural state'. Additional influencing factors of GW availability are the length of the growing season for biomass production, vegetation water demand and soil properties.

Regional differences in GW availability as a consequence of ALC conversion are depicted in figure 8b. While areas under heavy agricultural production in Europe and North America experienced a steep decline in GW availability, a slight increase in GW availability has been simulated in the wet-dry tropics and most noteably in the heavily agriculturaly transformed and irrigated Ganges and Indus river basins of the Indian subcontinent. It is important to bear in

mind that GW availability and soil moisture are not conterminus, higher GW availability does not necessarily imply higher soil moisture thoughout the entire soil column.

GW-flow efficiency (GW_{eff}):

Since GW_{eff} is a weighted ratio of transpiration, soil evaporation and interception loss, highest values are yielded in areas with a high overall GW-flow and where most of the GW-flow is made productive.

Under PNVr, the indicator yielded highest results in the humid tropics (figure 8c). The humid tropics are the engine of the water cycle due to the combination of high precipitation rates, high atmospheric water demands and dense vegetation coverage, leaving little space for soil evaporation. However, this tendency is partly balanced out by water being intercepted in the canopy which can thus not be made productive. On the contrary, GW-flow comes nearly to a halt in sparsely vegetated areas or areas with little liquid precipitation, such as the high latitudes or deserts.

Anthropogenic changes of GW_{eff} are mainly of a negative nature (figure 8d). Deforestation and the interlinked occurrence of prolongated fallow periods are favoring soil evaporation and thus entail a shift towards unproductive GW-flow, eventually lowering GW_{eff}. This tendency might be partly offset by irrigation. Areas, by and large covered with PNV today, are usually dominated by transpiration and thus yield higher GW_{eff} scores. In conclusion, deforestation in areas with high productive GW-flow is having the strongest impact on GW_{eff}.

Another factor that could potentially have a big impact on GW_{eff} are changes in precipitation. However, since precipitation is defined by the climate input, this factor is not considered within this study. For further information see Appendix B and C for productive and unproductive GW-flow and the human-induced changes to these parameters.

GW deficiency (L_{TA}):

The indicator for the ratio between actual and potential canopy conductance is given by Gerten et al. (2007) and indicates GW stress and thereby GW deficiency. The lower the experienced water stress, the smaller the gap between actual and potential canopy conductance.

Under PNVr (figure 8e), the GW limitation is lowest in the high altitudes and in the humid tropics, which is in agreement with previous results employing the indicator (Gerten et al. 2007). The rationale behind the signal is that in both zones water is rarely a growth limiting factor and has thereby little to no negative implications for photosynthesis and thereby CO_2 sequestration.

Human-induced changes in L_{TA}, as simulated within this study, are tremendous (figure 8f). Even though the changes in GW_{eff} (figure 8d) already imply a certain water deficiency and thereby an overall lowering of the L_{TA} indicator, the simulated changes in L_{TA} seem far from being realistic. Especially changes in the Congo basin, which has not experienced large scale ALC conversion (cf. figure 9), are unexplainable. One cause for the overestimation could stem from the fact that the L_{TA} has not yet been utilized with CFTs. An aggregation error within the model is therefore likely.

4.3 Regional plots

Changes in the green aspect of the water cycle can be seen in areas with extensive human land cover conversion (figure 9). In comparison with PNVr, the PFT coverage in grid cells highly shrunk as a consequence of CFT cultivation in the ALCr_irr (Appendix F).

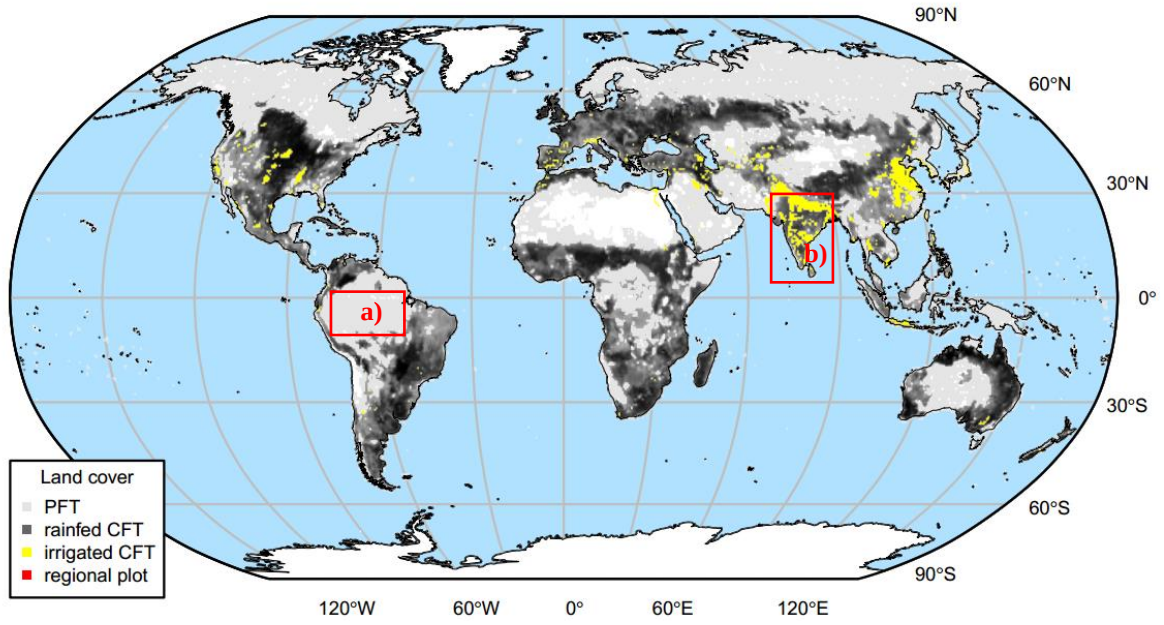

Figure 9. Global distribution of PFTs and CFTs under ALCr_irr. White areas are without vegetation, in light gray are grid cells occupied by at least 90% PFTs, the darkness of the gradual darker gray depicts the amount of CFT coverage. Black areas are therefore nearly entirely covered with CFTs. Yellow grid cells are covered by at least 10% irrigated CFTs. Red boxes show the spatial extent of regional plots shown below in figure 10.

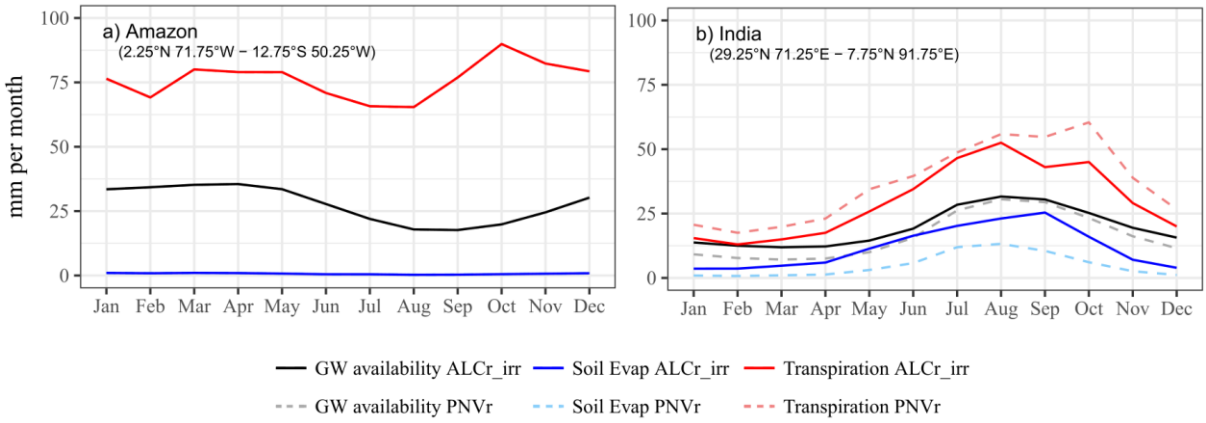

Figure 10. Intra-annual trends of GW_{avail}, E_{soil} and E_{transp} for PNVr and ALCc_irr in a) the Amazon basin and b) the Indian subcontinent. For the matter of clarity, only the mean values of the 30-year timeframe (1976-2005) were plotted, leaving out the interannual variability.

The Amazon basin and the Indian subcontinent were chosen to be examined in more detail due to their contrasting anthropogenic interferences as well as their consideration as GW-related tipping elements (chapter 2.4.4). While the chosen segment of the Amazon basin was nearly undisturbed in the simulated timeframe (1976 – 2005), the Indian subcontinent has been heavily transformed and irrigated (regional plots a and b in figure 9). The low ALC conversion rate within the core zone of the Amazon rainforest causes a nearly perfect agreement between PNVr and ALCr_irr (figure 10a). High natural vegetation density in the Amazon basin leaves very little space for bare soil, thereby causing very low soil evaporation rates. Transpiration, thus productive GW-flow, on the contrary, yields very high results throughout the year. The two peaks being simulated for productive GW-flow are most likely linked to higher precipitation values stemming from the seasonal variations of the Intertropical Convergence Zone. Interception was not plotted in figure 10 but yields among the highest values in Amazonia, compared against the rest of the world (Appendix C). Except the evaporation of intercepted precipitation, nearly all terrestrial water vapor stems from a productive, thus plant-based, pathway.

The Indian subcontinent, on the other hand, experienced a widespread ALC conversion, causing a strong shift in GW availability, soil evaporation and transpiration (figure 10b). In general, all three parameters show a strong intra-annual trendline, peaking during the high precipitation in the Indian summer monsoon. The following shifts can be seen as a consequence of anthropogenic interference. First, productive GW-flow, thus transpiration, declined consistently throughout the year with the highest losses during the monsoon. Second, soil evaporation gained tremendous flux volume, especially during the monsoon. This significant shift in GW-flow is well captured by the GW_{eff} indicator (cf. figure 8d). Lastly, GW availability increased especially during winter and early spring.

5. Discussion

5.1 The concept of green water

Sood et al. (2014) correctly argue that the water color terminology does not fill a terminological vacuum but simply assigns color-bonded words to already existing hydrological terminology, among others soil evaporation, transpiration and soil moisture. However, the demarcation between GW and BW is a powerful tool to shift the attention of policy makers and water management towards the ‘invisible’, yet highly important green aspects of the water cycle and thereby path the way for an incorporated land and water resources management (Falkenmark and Rockström 2006).

The non-uniform definitions of GW and GW-flow are cumbersome and an obstacle in applying the concept (Sood et al. 2014). The inconsistent definitions forced the authors of nearly every GW-related study, including this one, to redefine the concept to assure that no misunderstandings occur. This study has aimed at providing a more comprehensive definition as visualized in figure 2. One of the biggest obstacles to overcome was whether to limit GW to plant accessible GW only, as originally proposed by Falkenmark (1995). This, in turn, would

exclude unproductive GW-flow since neither evaporation of intercepted water nor from bare ground would be included in such a definition. Nevertheless, they play a central role in terrestrial moisture recycling (van der Ent et al. 2014) and must therefore be accounted for. Another discrepancy with earlier definitions arises from calling evaporation of intercepted precipitation and soil evaporation green, as they have previously been labelled as white water (Ringersma et al. 2003).
A major weakness of the proposed definition arises from the fact that only the moisture of the upper soil layer of the vadose zone is available for soil evaporation, deeper soil layers which are still above the groundwater table and are not within the rootzone of any vegetation, one could argue, can therefore be excluded in the definition of GW.

5.2 Results of the modelling study

Comparing the 'natural state' of terrestrial water balance (PNVr) with its condition in the 'actual state' (ALCr_irr), revealed significant changes among all green and blue water related parameters (figure 6). Anthropogenic interference with the ES, as has been simulated in the course of this study, constitutes a major force of change in the terrestrial water cycle. Individual aspects of human disturbances have been presented in the previous chapter and will be discussed in the following.

GW availability (GW_{avail}):
The combination of unchanged precipitation paired with a simultanous uniform increase in runoff and an almost unchaged overall GW-flow makes the slight overall increase in GW availability look surprising. In fact, a decrease in GW-stock replenishment with a simultaneous almost unchanged overall water loss towards the atmosphere (GW-flow) cause a decrease in overall soil moisture, as observations show for intensively cultivated areas in Northern China (Liu et al. 2015). However, a closer look into the spatial heterogenity can unveil potential solutions. A decrease in plant accessable GW, as being simulated in eastern North America and Central Europe, can potentially be explained by lower rooting depths and densities of CFTs as compared against the PFTs in the same area under PNVr, thereby accessing soil moisture to a lesser extent (figure 8b). The contrary trend can be wittnessed on the Indian subcontinent, where water in the rootzone yielded higher results under ALCr_irr than PNVr. One possible explanation could stem from the fact that ALC led to a reduction in productive GW-flow (figure 10b), thereby reducing the consumption of plant available GW. Another factor benefitting GW availability is irrigation. This claim is supported by the fact that biggest increases in GW availability are simulated for the Ganga and Indus river basins on the Indian subcontinent which are heaviliy irrigated (cf. figure 9, 10b).

GW-flow:
Anthropogenic interferences with the water cycle changed overall GW-flow as well as its composition. By the same token, it is important to note that GW-flow values differ highly between different PFTs and CFTs (a list can be found under Rockström et al. 1999) which the chosen model output format fails to resolve. However, the aim of the study did not require a

band-based, but a cell mean resolution, since a cell-based presentation of the data (e.g. via maps) requires cell-based mean values.
In general, global terrestrial water vapor flux estimations und ALC (GW-flow in table 4) are within the range of prior estimations of 63,000-72,500 km³ yr^{-1}. Nevertheless, anthropogenic land use affects the overall GW-flow in two contrary directions. Deforestation, on the one hand, resulted in an overall reduction in GW, returning less water to the atmosphere, thereby favoring a moisture recycling deceleration (figure 4a, 7a). Redirecting runoff for field irrigation, on the other hand, led to an increase in GW-flow and is, by returning more water to the atmosphere, benefiting moisture recycling acceleration (figure 4b, 7b). Despite stark regional differences, these two trends are nearly offsetting each other on a global level resulting in a neglectable change of total GW-flow due to ALC conversion. This finding is in accordance with previous studies (Gordon et al. 2005).

GW-flow efficiency (GW_{eff}):
In order to depict the aforementioned change from productive to unproductive GW-flow as a result of ALC, the GW_{eff}-indicator has been introduced (chapter 3.3). GW_{eff} allows to surface a shift from productive to unproductive GW-flow and vice-versa. The conducted simulation points towards an almost consistent reduction of GW_{eff} in areas of intensive agricultural production (figure 8d, compare with figure 9). This claim is supported by the fact that the amount of transpired water declined while soil evaporation rates increased, causing a shift from productive to unproductive GW-flow on a global scale (figure 6 and table 4). Even though it was not explicitly tested within this study, it is very likely that GW-flow became less and less productive with the successive historical agricultural expansion as being stated by Gerten et al. (2005). This finding is well-aligned with prior reports stating that deforestation decreased transpiration rates while fallowness increases the soil evaporation rates of the same patch (Baron et al. 1998; Zhang et al. 2014). A decrease in productive GW-flow directly correlates with net primary production (Chen and Coughenour 2004). Furthermore, the reduced and seasonalized vegetation stand of agricultural land in comparison with forest biomes leads to a reduction in interception and thus dampens the shift towards unproductive GW-flow since more precipitation is reaching the soil surface. Another cause of the shift is the shorter growing seasons under anthropogenic land cover when compared against a PNV stand. It is likely that transpiration rates under ALC are comparable with or even outrun PNV values during the growing season but experienced a steep decline outside of the growing season, since land surfaces lay fallow in between agricultural production cycles, as can be seen for the timelines in Europe (Appendix G). The regional plot of the Indian subcontinent (figure 10b) breaks down the significant decline in GWeff for the area (figure 8d). All in all, the simulated reduction in transpiration and interception is consistent with earlier modelling studies (Rost et al. 2008b).
However, the extent of changes in transpiration, interception and soil evaporation are significantly underestimated in comparison with previous studies. Global transpiration declined only by 603 km³ yr^{-1} (1.13%) and soil evaporation increased by 510 km³ yr^{-1} (5.75%), while a decline of 7.4% and an increase of 9.7% have been reported for transpiration and evaporation, respectively (Gerten et al. 2005). A plausible explanation for this mismatch stems from the fact that the LPJmL4 output of GW related parameters have been written as mean values per grid cell, not per PFT/CFT band, thus offsetting potential de- and increases of

transpiration and evaporation, respectively, within each grid cell. A list of GW resources consumed by different biomes can be found under Rost et al. (2008a).
Regional differences of GW-flow components will not be elaborated individually as they are aggregated in GW_{eff}. However, individual maps can be found in the appendix (Appendix B and C). Nevertheless, changes in GW-flow composition have, in turn, implications on moisture recycling. By employing an atmospheric moisture tracking model, van der Ent et al. (2014) were able to show that moisture originating from different GW-flow pathways was characterized by different atmospheric residence times and transportation distances. The recirculation of GW taking the productive GW-flow pathway is delayed compared against the unproductive pathway, especially evaporation of intercepted precipitation, since transpired water must be taken up by the plants in the first place. A better knowledge of anthropogenic perturbations on individual GW-flow components must be obtained. This holds particularly true for global simulation studies, since comprehensive studies studying the land-use signature on GW-flow composition are sparse Rost et al. (2008b).

GW deficiency (L_{TA}):
GW deficiency cannot be accounted for with GW_{eff} since the indicator fails to depict GW demand and thereby to what extent transpiration, and thus photosynthesis, are GW-limited. The L_{TA} indicator as introduced by Gerten et al. (2007), bears the potential to fill the gap as has been elaborated in chapter 3.3. Employing L_{TA} within this study would therefore be more suitable for the proposed research question, however, since L_{TA} has not yet been optimized for CFTs, the given results should be considered at most preliminary (figure 8f). Any human-induced drop of the indicator implies a aggravated water limitation of photosynthesis and thereby the CO_2 capture capacity of the biosphere, with detrimental effects on the Climate Change mitigation potential of the biosphere (Humphrey et al. 2018)

Major results of the modelling study are:

i. GW availability increased slightly under ALC (with irrigation)
ii. Increased runoff leads to an extended BW availability
iii. The total terrestrial water vapor flux changed insignificantly but the composition shifted strongly towards unproductive GW-flow with implications for net primary production and CO_2 sequestration in vegetation
iv. The introduced GW indicator GW_{eff} can depict the shift in GW-flow composition

Every model is a rough simplification of reality, accompanied with a large set of assumptions and generalizations. A model capable of dynamically accounting for global vegetation and interlinked biogeochemical and water fluxes as a response to external forcing is certainly constrained by a set of limitations. In the context of GW, LPJmL4 lacks a representation of agricultural soil compaction and a subsequent reduction in infiltration (Nawaz et al. 2013), as well as surface sealing.
A drawback of the conducted modelling study was the chosen timeframe (average of 1976-2005) since ongoing land cover changes since the year 2005 might have yielded different results. Moreover, the average of the standardized length of 30 years is weakening the signal

of recent changes. Comparing the results of this study against earlier estimates yields a big mismatch in transpiration and soil evaporation (Rost et al. 2008b in table 4). However, considering the differences in the simulated timeframe, LPJmL model version and climate input data, makes the results barely comparable.

5.3 Implementing green water in the Planetary Boundary for Freshwater use

5.3.1 The green gap

Even though green water and the interlinked risks of human perturbations have already been discussed in the original version of the PB framework, runoff depletion, thus BW instead of GW, was chosen to constitute the planetary CV (Rockström et al. 2009b). This decision builds on the assumption that GW and BW are intricately linked (Rockström et al. 2009; supplementary information). Increased GW-flow, according to the reasoning, would lead to less runoff and percolation but higher precipitation. A reduced GW-flow, on the other hand, decelerates moisture recycling and therefore reduces precipitation, in turn diminishing BW formation. Changes in consumptive BW use, on the contrary, could affect moisture recycling due to the evaporation of redirected runoff (irrigation) and water vapor flux from open waters. The latter process has not been accounted for within this study. However, the results of the conducted modelling study point towards very strong global implications of ALC and thereby GW appropriation for runoff and discharge (appendix D and E), but only relatively minor and regional implications of irrigation on GW (figure 6 left vs. right, appendix B, C and D). Nonetheless, redirected BW almost cancels out the deforestation-induced GW-flow (Gordon et al. 2005). This argumentation confirms the assumption by Rockström et al. (2009b) that GW and BW are intricately linked and changes in one part of the terrestrial water cycle have implications on another, especially when considering the terrestrial-atmosphere moisture recycling. However, the argumentation further poses the question why BW and not GW has been used to derive CVs monitoring the state of the PB-W in the first place, since interferences with GW lead to changes in BW. At the current point, the status quo is implicitly assuming that the two BW CVs (both global and subglobal) aggregate BW and GW in a sufficient manner (Gerten et al. 2015; Steffen et al. 2015b). In fact, even though the PB-W is currently defined by an upper limit in BW consumption, crossing the PB-W would imply to *'significantly increase the risk of approaching green and blue water-induced thresholds (collapse of terrestrial and aquatic ecosystems, major shifts in moisture feedback, and freshwater/ocean mixing)'*(Rockström et al. 2009b). As a consequence, the PB-W, thus the upper limit of human interference with the water cycle, has to be set to *guarantee 'enough green water flows for moisture feedback (to regenerate precipitation), allow for the provisioning of terrestrial ecosystem functioning and services (e.g., carbon sequestration, biomass growth, food production, and biological diversity), and secure the availability of blue water resources for aquatic ecosystems'* (Rockström et al. 2009b). This assumption builds on the blurry premise that all human interferences with GW lead to changes in BW. GW_{eff} calls evidence in rebuttal of this claim by surfacing that even though the overall GW-flow did not change significantly as a consequence of ALC, the proportion of different GW-flow pathways did, with crucial

consequences on CO_2 sequestration (Humphrey et al. 2018), net primary production (Chen and Coughenour 2004) and moisture recycling (van der Ent et al. 2014). Human-induced changes in ALC interfere with the well-functioning of the ES but do not leave a clear trace in BW downstream. One could subsequently argue that monitoring the status of PB-W exclusively by BW-based CVs is insufficient. This claim is in accordance with the scientific debate regarding the definition of PB-W. Heistermann (2017) justifiably argued that if *'the disruption of terrestrial moisture recycling is considered crucial, then the boundary should be redefined accordingly, including an explicit acknowledgement of our fundamental gaps in qualitative and quantitative understanding'*. The contribution of this thesis to partly fill this gap will be summarized in the following.

5.3.2 A green water-based control variable

A dedicated CV to account for green water within the Planetary boundary framework would be vital to measure, monitor and visualize human perturbations of GW on the one hand as well as setting an upper limit to the GW perturbations with respect to the well-functioning of the ES on the other hand. Rockström et al. (2009b) stated that the positioning of any PB should follow the precautionary principle and be therefore either 'well below' (i) reaching a potential threshold of non-linear tipping points or (ii) increasing the likelihood of reaching tipping points of other PBs.

In the context of GW, both principles are viable. On the one hand can human-induced changes in moisture supply in the Amazon basin and the Indian subcontinent lead to a self-amplified deceleration of the moisture feedback, thereby heralding the start of non-linear regime shifts, thus tipping points towards dryer conditions. Even though other influencing factors, such as higher temperature under climate change, atmospheric aerosol loading or changes in albedo are seen as major forcing, deforestation and thereby ALC interference with GW can contribute to such a transition in the Amazon (Zemp et al. 2017; Weng et al. 2018) and the Indian summer monsoon (Pathak et al. 2014). On the other hand, an overexploitation of GW resources can increase the likelihood of reaching tipping points within other PBs. As has been elaborated above, global decreases in soil moisture supply led to a subsequent growth of atmospheric CO_2 (Humphrey et al. 2018), thereby aggravating the status of the Climate change-PB.

An individual PB for GW, however, does not seem plausible, given that GW and BW are intricately linked and human modifications in GW are the consequence of GW appropriation for the production of commodities (predominantly rainfed agriculture and forestry), thus freshwater use. In short, GW needs to be accounted for within the PB-W (figure 11).

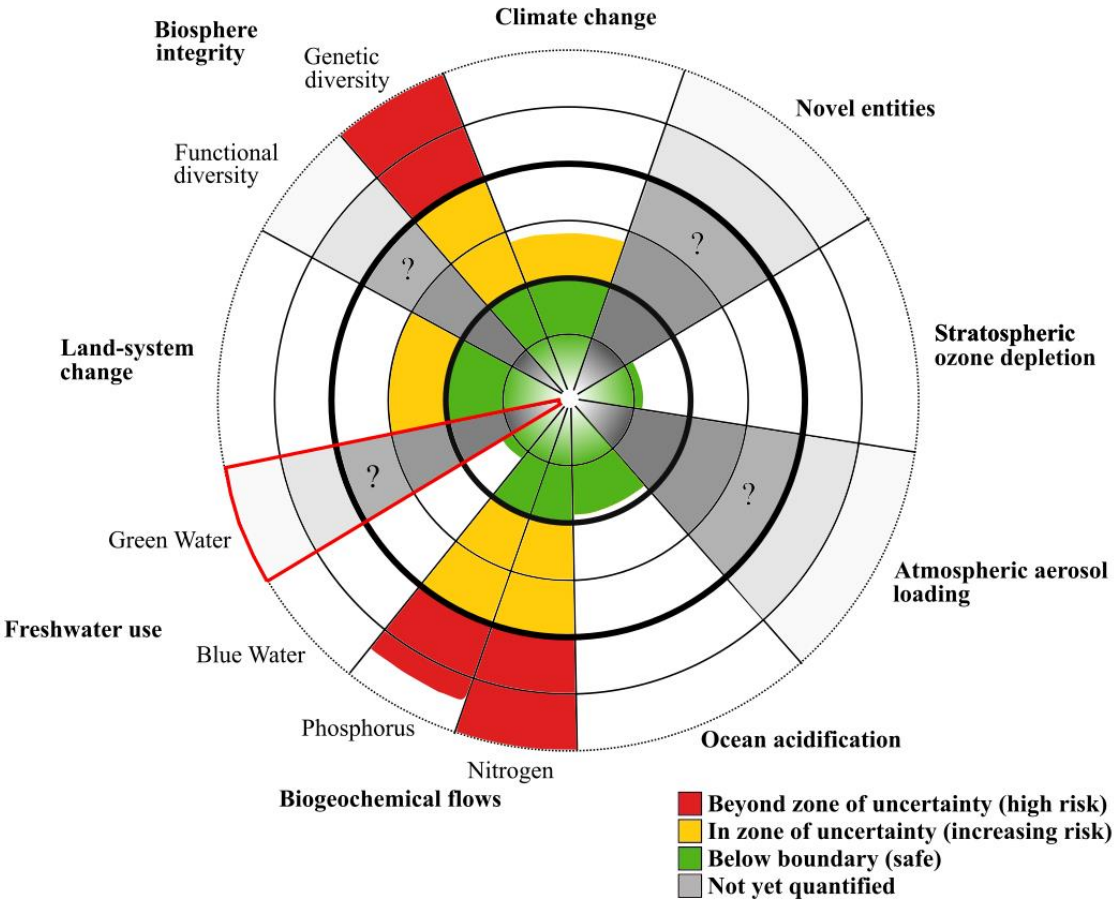

Figure 11. Updated Planetary Boundaries framework; Same as figure 1, but the Planetary Boundary for Freshwater use has been extended and now accounts for the still unknown state of a control variable for green water (red triangle).

Heistermann (2017) accentuated fundamental qualitative and quantitative gaps concerning the incorporation of GW within the PB-W. As elaborated above, a dedicated CV for GW appears rational and an exposition of the qualitative and quantitative basis for it will be elaborated below.

Qualitative fundament. Given the strong regional operating scale of moisture recycling and GW-related tipping points, a subglobal CV would be a more suitable way to monitor human perturbations of GW than a global operating one. A CV would need to be capable of monitoring the following criteria:

i. that GW-flow supplies sufficient moisture to the atmosphere to maintain crucial local and trans-regional moisture recycling
ii. that enough GW is both plant-available and made productive by plants to prevent large-scale and consistent GW stress in the biosphere and thereby alleviate the biospheres' CO_2 capture capacities
iii. the reaching of GW-related tipping points in the ES

As has been demonstrated by van der Ent et al. (2010), the contribution of regional and continental moisture recycling differs vastly around the globe. Based on the example of the Amazon basin, Weng et al. (2018) were further able to show that MIPs need to be detected even inside these highly contributing areas, since downwind precipitation is particularly sensitive towards GW-flow changes in MIPs. In summary, MIPs for core source areas of terrestrial water vapor flux need to be identified and contributed for within a CV for GW. This holds especially true for regional moisture recycling within tipping elements.

Quantitative fundament. From a landscape perspective, a minimum regional GW-flow in MIPs need to be maintained in order to guarantee sufficient humidity supply to sustain regional and continental moisture recycling. Moreover, it has to be made sure that a certain fraction of GW-flow takes the productive pathway of transpiration in order to sustain biophysical processes, CO_2 sequestration and net primary production. Anthropogenic changes in GW-flow as expressed by the GW_{eff} indicator can hereby be taken as a preliminary result, highlighting local changes in overall GW-flow and GW-flow composition (figure 12). Note that the subglobal boundaries as expressed in figure 12 are scientifically unfounded and serve for illustration purposes only. It is a preliminary draft. In summary, a global aggregate of spatiotemporally specific GW-flow values, under consideration of the GW-flow composition, for each MIP could be the way forward. Similar to the environmental flow requirements of river systems (Gerten et al. 2013), a minimum of required productive and overall GW-flow within each MIP can act as the major determent of the GW CV.

Draft of a subglobal CV for GW, based on GW_{eff}:

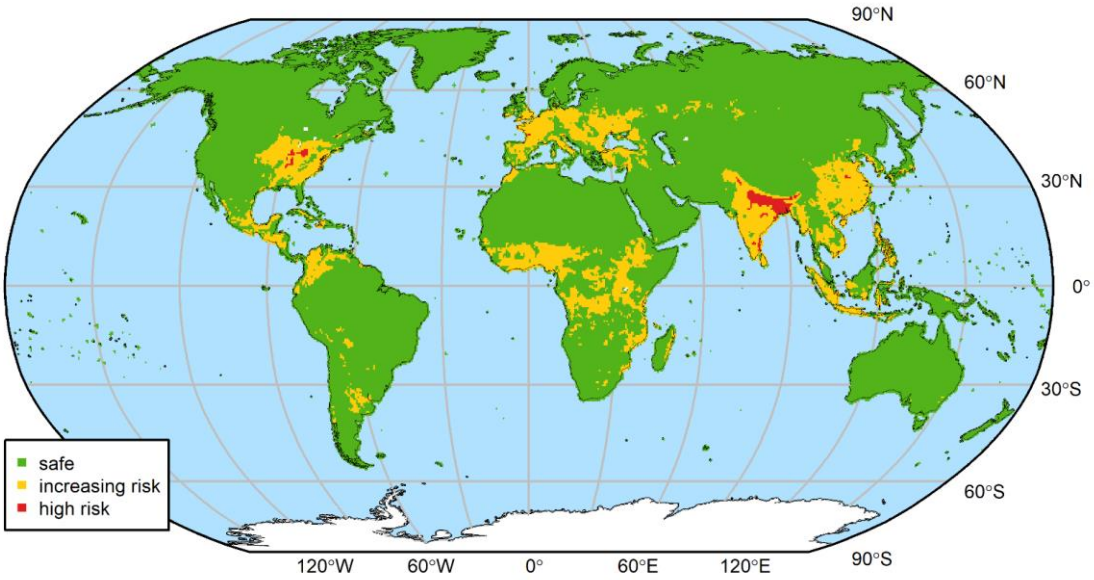

Figure 12. GW_{eff} -based preliminary draft of a subglobal control variable, depicting transgression of a potential GW CV within PB-W as a consequence of ALC transfromation. Areas in green represent areas with minor negative and positive changes (-0.005, max) in GW_{eff}, areas in yellow represent zones with increasing risks (-0.07,-0.005) and areas in red show a high risk (min,-0.07)

6. Conclusions and outlook

The conducted modelling study unveiled large-scale perturbations of the terrestrial water cycle due to anthropogenic land cover transformations. Even though the global total of the terrestrial water vapor flux did barely change, anthropogenic perturbations led to the antagonistic effects of deforestation and irrigation, whose contrary effects on terrestrial water vapor flow are nearly offsetting each other on a global scale but amplify spatial heterogeneities.
Accentuated changes were simulated for the internal composition of the green water flux between the terrestrial surface and the atmosphere. While productive green water flow, that is water transpired during CO_2 uptake to maintain photosynthesis, declined substantially, unproductive green water flow, that is unused purely physical evaporation, increased proportionately. The introduced GW_{eff} indicator succeeded in depicting the shift towards an overall decreased green water flow efficiency as a consequence of land cover conversion. This shift is alarming due to the vital role that green water plays within the complex Earth system. Plant accessible green water sustains basic biophysical processes of the terrestrial biosphere and relies on a constant replenishment via precipitation. Atmospheric moisture leading to precipitation, in turn, is replenished by terrestrial water fluxes. This mutual interdependency is known as moisture recycling and can easily be disrupted by anthropogenic land-use and subsequent changes in the terrestrial water cycle. The sustainment of these atmospheric rivers is especially sensitive towards land-use changes in the most important core precipitationsheds, that are moisture source areas contributing immensely to regional or continental moisture recycling. In addition, the Amazon rainforest, the Indian summer monsoon as well as the West African monsoon are considered as tipping elements in the Earth system. Their tipping behavior is at least partly dependent on moisture supply originating from terrestrial sources and records attest partial regime shifts within these tipping elements during the Holocene.
Nonetheless, a safe operating space of anthropogenic interference of green water is currently not been accounted for within the Planetary Boundary for Freshwater use, which is seen as a major weakness of its current definition. This study has been a first attempt in providing a qualitative and quantitative fundament of a dedicated control variable to account for green water within the Planetary Boundary for Freshwater use.

Novel findings of the study are:

i. GW_{eff} – a new green water indicator successfully depicted changes in the composition of green water flow
ii. A conceptualized qualitative and quantitative fundament for implementing green water into the Planetary Boundary for Freshwater use via a dedicated subglobal control variable for green water

Future research aiming at implementing a green water control variable should focus on:

i. Identification of the most important precipitationsheds as the core source areas of terrestrial water vapor flux to sustain regional and continental moisture recycling, especially within green water-related tipping elements
ii. Quantification of the minimum terrestrial water vapor flow requirements for each core precipitationshed to sustain crucial moisture recycling
iii. Improvement of the understanding of the impact on individual green water flow pathways and their subsequent roles in moisture recycling
iv. Implementation of a green water deficiency indicator (e.g. L_{TA}) to quantify the loss of CO_2 sequestration in vegetation as a function of green water stress
v. Analysis of key interactions between green water and other Planetary Boundaries, e.g. climate change or land-system change.

References

Allen, M. 2009. Planetary boundaries: Tangible targets are critical. *Nature Reports Climate Change*, 3**:** 114-115. DOI: 10.1038/climate.2009.95

Arguez, A., and R. S. Vose. 2011. The Definition of the Standard WMO Climate Normal The Key to Deriving Alternative Climate Normals. *Bulletin of the American Meteorological Society,* 92**:** 699-704. DOI: 10.1175/2010bams2955.1

Barnosky, A. D., E. A. Hadly, J. Bascompte, E. L. Berlow, J. H. Brown, M. Fortelius, W. M. Getz, J. Harte, et al. 2012. Approaching a state shift in Earth's biosphere. *Nature*, 486**:** 52-58. DOI: 10.1038/nature11018

Baron, J. S., M. D. Hartman, T. G. F. Kittel, L. E. Band, D. S. Ojima, and R. B. Lammers. 1998. Effects of land cover, water redistribution, and temperature on ecosystem processes in the South Platte Basin. *Ecological Applications,* 8**:** 1037-1051. DOI: 10.2307/2640959

Baumgartner, A., and E. Reichel. 1975. *Die Weltwasserbilanz*. Munich, Vienna: R. Oldenbourg Verlag.

Bondeau, A., P. C. Smith, S. Zaehle, S. Schaphoff, W. Lucht, W. Cramer, D. Gerten, H. Lotze-Campen, et al. 2007. Modelling the role of agriculture for the 20th century global terrestrial carbon balance. *Global Change Biology,* 13**:** 679-706. DOI: 10.1111/j.1365-2486.2006.01305.x

Boone, A. A., Y. K. Xue, F. De Sales, R. E. Comer, S. Hagos, S. Mahanama, K. Schiro, G. Q. Song, et al. 2016. The regional impact of Land-Use Land-cover Change (LULCC) over West Africa from an ensemble of global climate models under the auspices of the WAMME2 project. *Climate Dynamics,* 47**:** 3547-3573. DOI: 10.1007/s00382-016-3252-y

Bosch, J. M., and J. D. Hewlett. 1982. A Review of Catchment Experiments to Determine the Effect of Vegetation Changes on Water Yield and Evapo-Transpiration. *Journal of Hydrology,* 55**:** 3-23. DOI: 10.1016/0022-1694(82)90117-2

Bowen, G. J. 2011. A faster water cycle. *Science,* 332**:** 430-431. DOI: 10.1126/science.1205253

Chen, D.-X., and M. B. Coughenour. 2004. Photosynthesis, transpiration, and primary productivity: Scaling up from leaves to canopies and regions using process models and remotely sensed data. *Global Biogeochemical Cycles,* 18**:** GB4033. DOI: 10.1029/2002GB001979

de Fraiture, C., and D. Wichelns. 2010. Satisfying future water demands for agriculture. *Agricultural Water Management,* 97**:** 502-511. DOI: 10.1016/j.agwat.2009.08.008

Dirmeyer, P. A., and K. L. Brubaker. 2007. Characterization of the Global Hydrologic Cycle from a Back-Trajectory Analysis of Atmospheric Water Vapor. *Journal of Hydrometeorology,* 8**:** 20-37. DOI: 10.1175/jhm557.1

Dixit, Y., D. A. Hodell, R. Sinha, and C. A. Petrie. 2014. Abrupt weakening of the Indian summer monsoon at 8.2 kyr B.P. *Earth and Planetary Science Letters,* 391**:** 16-23. DOI: 10.1016/j.epsl.2014.01.026

Eltahir, E. A., and R. L. Bras. 1994. Precipitation recycling in the Amazon basin. *Quarterly Journal of the Royal Meteorological Society,* 120**:** 861–880.

Falkenmark, M. 1995. Coping with water scarcity under rapid population growth. In *Conference of SADC Ministers*. Pretoria, South Africa.

Falkenmark, M., and J. Rockström. 2004. *Balancing Water for Humans and Nature: The New Approach in Ecohydrology*. London: Earthscan.

Falkenmark, M., and J. Rockström. 2006. The new blue and green water paradigm: Breaking new ground for water resources planning and management. *Journal of Water Resources Planning and Management-Asce,* 132**:** 129-132. DOI: 10.1061/(Asce)0733-9496(2006)132:3(129)

Falkenmark, M., L. Wang-Erlandsson, and J. Rockström. 2019. Understanding of water resilience in the Anthropocene. *Journal of Hydrology X,* 2**:** 100009. DOI: 10.1016/j.hydroa.2018.100009

Frieler, K., S. Lange, F. Piontek, C. P. O. Reyer, J. Schewe, L. Warszawski, F. Zhao, L. Chini, et al. 2017. Assessing the impacts of 1.5 °C global warming – simulation protocol of the Inter-Sectoral Impact Model Intercomparison Project (ISIMIP2b). *Geoscientific Model Development,* 10**:** 4321-4345. DOI: 10.5194/gmd-10-4321-2017

Gaetani, M., G. Messori, Q. Zhang, C. Flamant, and F. S. R. Pausata. 2017. Understanding the Mechanisms behind the Northward Extension of the West African Monsoon during the Mid-Holocene. *Journal of Climate,* 30**:** 7621-7642. DOI: 10.1175/Jcli-D-16-0299.1

Gerten, D., H. Hoff, A. Bondeau, W. Lucht, P. Smith, and S. Zaehle. 2005. Contemporary "green" water flows: Simulations with a dynamic global vegetation and water balance model. *Physics and Chemistry of the Earth,* 30**:** 334-338. DOI: 10.1016/J.Pce.2005.06.002

Gerten, D., H. Hoff, J. Rockström, J. Jägermeyr, M. Kummu, and A. V. Pastor. 2013. Towards a revised planetary boundary for consumptive freshwater use: role of environmental flow requirements. *Current Opinion in Environmental Sustainability,* 5**:** 551-558. DOI: 10.1016/j.cosust.2013.11.001

Gerten, D., J. Rockström, J. Heinke, W. Steffen, K. Richardson, and S. Cornell. 2015. Response to Comment on "Planetary boundaries: Guiding human development on a changing planet". *Science,* 348**:** 1217. DOI: 10.1126/science.aab0031

Gerten, D., S. Schaphoff, U. Haberlandt, W. Lucht, and S. Sitch. 2004. Terrestrial vegetation and water balance—hydrological evaluation of a dynamic global vegetation model. *Journal of Hydrology,* 286**:** 249-270. DOI: 10.1016/j.jhydrol.2003.09.029

Gerten, D., S. Schaphoff, and W. Lucht. 2007. Potential future changes in water limitations of the terrestrial biosphere. *Climatic Change,* 80**:** 277-299. DOI: 10.1007/s10584-006-9104-8

Gordon, L., M. Dunlop, and B. Foran. 2003. Land cover change and water vapour flows: learning from Australia. *Philosophical Transactions of the Royal Society of London. Series B: Biological Sciences,* 358**:** 1973-1984. DOI: 10.1098/rstb.2003.1381

Gordon, L. J., W. Steffen, B. F. Jonsson, C. Folke, M. Falkenmark, and A. Johannessen. 2005. Human modification of global water vapor flows from the land surface. *Proceedings of the National Academy of Sciences,* 102**:** 7612-7617. DOI: 10.1073/pnas.0500208102

Gupta, A. K., D. M. Anderson, and J. T. Overpeck. 2003. Abrupt changes in the Asian southwest monsoon during the Holocene and their links to the North Atlantic Ocean. *Nature,* 421**:** 354. DOI: 10.1038/nature01340

Heistermann, M. 2017. HESS Opinions: A planetary boundary on freshwater use is misleading. *Hydrology and Earth System Sciences,* 21**:** 3455-3461. DOI: 10.5194/hess-21-3455-2017

Held, I. S., and B. J. Soden. 2000. Water Vapor Feedback and Global Warming. *Annual Review of Energy and the Environment,* 25**:** 441–475.

Hirota, M., M. Holmgren, E. H. Van Nes, and M. Scheffer. 2011. Global Resilience of Tropical Forest and Savanna to Critical Transitions. *Science,* 334**:** 232-235. DOI: 10.1126/science.1210657

Hoekstra, A. Y., M. M. Mekonnen, A. K. Chapagain, R. E. Mathews, and B. D. Richter. 2012. Global monthly water scarcity: blue water footprints versus blue water availability. *PLoS One,* 7**:** e32688. DOI: 10.1371/journal.pone.0032688

Humphrey, V., J. Zscheischler, P. Ciais, L. Gudmundsson, S. Sitch, and S. I. Seneviratne. 2018. Sensitivity of atmospheric CO2 growth rate to observed changes in terrestrial water storage. *Nature,* 560**:** 628-631. DOI: 10.1038/s41586-018-0424-4

Jaramillo, F., and G. Destouni. 2014. Developing water change spectra and distinguishing change drivers worldwide. *Geophysical Research Letters,* 41**:** 8377-8386. DOI: 10.1002/2014gl061848

Jaramillo, F., and G. Destouni. 2015. Comment on "Planetary boundaries: Guiding human development on a changing planet". *Science,* 348**:** 1217. DOI: 10.1126/science.aaa9629

Jung, M., M. Reichstein, P. Ciais, S. I. Seneviratne, J. Sheffield, M. L. Goulden, G. Bonan, A. Cescatti, et al. 2010. Recent decline in the global land evapotranspiration trend due to limited moisture supply. *Nature,* 467**:** 951-954. DOI: 10.1038/nature09396

Keys, P. W., E. A. Barnes, R. J. van der Ent, and L. J. Gordon. 2014. Variability of moisture recycling using a precipitationshed framework. *Hydrology and Earth System Sciences,* 18**:** 3937-3950. DOI: 10.5194/hess-18-3937-2014

Keys, P. W., R. J. van der Ent, L. J. Gordon, H. Hoff, R. Nikoli, and H. H. G. Savenije. 2012. Analyzing precipitationsheds to understand the vulnerability of rainfall dependent regions. *Biogeosciences,* 9**:** 733-746. DOI: 10.5194/bg-9-733-2012

Keys, P. W., L. Wang-Erlandsson, and L. J. Gordon. 2016. Revealing Invisible Water: Moisture Recycling as an Ecosystem Service. *PLoS One,* 11**:** e0151993. DOI: 10.1371/journal.pone.0151993

Kriebel, D., J. Tickner, P. Epstein, J. Lemons, R. Levins, E. L. Loechler, M. Quinn, R. Rudel, et al. 2001. The precautionary principle in environmental science. *Environmental Health Perspectives,* 109**:** 871-876. DOI: 10.2307/3454986

Lenton, T. M., H. Held, E. Kriegler, J. W. Hall, W. Lucht, S. Rahmstorf, and H. J. Schellnhuber. 2008. Tipping elements in the Earth's climate system. *Proceedings of the National Academy of Sciences,* 105**:** 1786-1793. DOI: 10.1073/pnas.0705414105

Lenton, T. M., and H. T. Williams. 2013. On the origin of planetary-scale tipping points. *Trends in Ecology & Evolution,* 28**:** 380-382. DOI: 10.1016/j.tree.2013.06.001

Lewis, S. L. 2012. We must set planetary boundaries wisely. *Nature,* 485**:** 417-417. DOI: 10.1038/485417a

Liu, Y., Z. Pan, Q. Zhuang, D. G. Miralles, A. J. Teuling, T. Zhang, P. An, Z. Dong, et al. 2015. Agriculture intensifies soil moisture decline in Northern China. *Scientific Reports,* 5**:** 11261. DOI: 10.1038/srep11261

Mayle, F. E., D. J. Beerling, W. D. Gosling, and M. B. Bush. 2004. Responses of Amazonian ecosystems to climatic and atmospheric carbon dioxide changes since the last glacial maximum. *Philosophical Transactions of the Royal Society B-Biological Sciences,* 359**:** 499-514. DOI: 10.1098/rstb.2003.1434

Meybeck, M. 2003. Global analysis of river systems: from Earth system controls to Anthropocene syndromes. *Philosophical Transactions of the Royal Society of London. Series B: Biological Sciences,* 358**:** 1935-1955. DOI: 10.1098/rstb.2003.1379

Molden, D. 2009. The devil is in the detail. *Nature Reports Climate Change,* 3**:** 116-117. DOI: 10.1038/climate.2009.97

Nachtergaele, F., H. van Velthuizen, L. Verelst, N. Batjes, K. Dijkshoorn, V. van Engelen, G. Fischer, A. Jones, et al. 2009. Harmonized world soil database. Food and Agriculture Organization of the United Nations.

Nawaz, M. F., G. Bourrié, and F. Trolard. 2013. Soil compaction impact and modelling. A review. *Agronomy for Sustainable Development,* 33**:** 291-309. DOI: 10.1007/s13593-011-0071-8

Nepstad, D. C., C. M. Stickler, B. Soares, and F. Merry. 2008. Interactions among Amazon land use, forests and climate: prospects for a near-term forest tipping point. *Philosophical Transactions of the Royal Society B-Biological Sciences,* 363**:** 1737-1746. DOI: 10.1098/rstb.2007.0036

Novick, K., R. Oren, P. Stoy, J.-Y. Juang, M. Siqueira, and G. Katul. 2009. The relationship between reference canopy conductance and simplified hydraulic architecture. *Advances in Water Resources,* 32**:** 809-819. DOI: 10.1016/j.advwatres.2009.02.004

Pathak, A., S. Ghosh, and P. Kumar. 2014. Precipitation Recycling in the Indian Subcontinent during Summer Monsoon. *Journal of Hydrometeorology,* 15**:** 2050-2066. DOI: 10.1175/jhm-d-13-0172.1

Patricola, C. M., and K. H. Cook. 2007. Dynamics of the West African Monsoon under Mid-Holocene Precessional Forcing: Regional Climate Model Simulations. *Journal of Climate,* 20**:** 694-716. DOI: 10.1175/jcli4013.1

Ringersma, J., N. Batjes, and D. Dent, 2003. Green Water: definitions and data for assessment. ISRIC – World Soil Information Report 2003/2, Wageningen. [in Swedish, English summary]

Rockström, J., M. Falkenmark, T. Allan, C. Folke, L. Gordon, A. Jagerskog, M. Kummu, M. Lannerstad, et al. 2014. The unfolding water drama in the Anthropocene: towards a resilience-based perspective on water for global sustainability. *Ecohydrology,* 7**:** 1249-1261. DOI: 10.1002/eco.1562

Rockström, J., M. Falkenmark, L. Karlberg, H. Hoff, S. Rost, and D. Gerten. 2009a. Future water availability for global food production: The potential of green water for increasing resilience to global change. *Water Resources Research,* 45. DOI: 10.1029/2007WR006767

Rockström, J., L. Gordon, C. Folke, M. Falkenmark, and M. Engwall. 1999. Linkages among water vapor flows, food production, and terrestrial ecosystem services. *Conservation Ecology* 3**:** 5.

Rockström, J., M. Lannerstad, and M. Falkenmark. 2007. Assessing the water challenge of a new green revolution in developing countries. *Proceedings of the National Academy of Sciences,* 104**:** 6253-6260. DOI: 10.1073/pnas.0605739104

Rockström, J., W. Steffen, K. Noone, A. Persson, F. S. Chapin, E. Lambin, T. M. Lenton, M. Scheffer, et al. 2009b. Planetary Boundaries: Exploring the Safe Operating Space for Humanity. *Ecology and Society,* 14**:** 32.

Rockström, J., W. Steffen, K. Noone, A. Persson, F. S. Chapin, E. F. Lambin, T. M. Lenton, M. Scheffer, et al. 2009c. A safe operating space for humanity. *Nature,* 461**:** 472-475. DOI: 10.1038/461472a

Rost, S., D. Gerten, A. Bondeau, W. Lucht, J. Rohwer, and S. Schaphoff. 2008a. Agricultural green and blue water consumption and its influence on the global water system. *Water Resources Research,* 44. DOI: 10.1029/2007WR006331

Rost, S., D. Gerten, and U. Heyder. 2008b. Human alterations of the terrestrial water cycle through land management. *Advances in Geosciences,* 18**:** 43-50. DOI: 10.5194/adgeo-18-43-2008

Savenije, H. H. G. 2000. Water scarcity indicators; the deception of the numbers. *Physics and Chemistry of the Earth Part B-Hydrology Oceans and Atmosphere,* 25**:** 199-204. DOI: 10.1016/S1464-1909(00)00004-6

Schaphoff, S., W. von Bloh, A. Rammig, K. Thonicke, H. Biemans, M. Forkel, D. Gerten, J. Heinke, et al. 2018. LPJmL4 – a dynamic global vegetation model with managed land – Part 1: Model description. *Geoscientific Model Development,* 11**:** 1343-1375. DOI: 10.5194/gmd-11-1343-2018

Scheffer, M., J. Bascompte, W. A. Brock, V. Brovkin, S. R. Carpenter, V. Dakos, H. Held, E. H. van Nes, et al. 2009. Early-warning signals for critical transitions. *Nature,* 461**:** 53-59. DOI: 10.1038/nature08227

Scheffer, M., S. Carpenter, J. A. Foley, C. Folke, and B. Walker. 2001. Catastrophic shifts in ecosystems. *Nature,* 413**:** 591-596. DOI: Doi 10.1038/35098000

Schyns, J. F., A. Y. Hoekstra, and M. J. Booij. 2015. Review and classification of indicators of green water availability and scarcity. *Hydrology and Earth System Sciences,* 19**:** 4581-4608. DOI: 10.5194/hess-19-4581-2015

Sitch, S., B. Smith, I. C. Prentice, A. Arneth, A. Bondeau, W. Cramer, J. O. Kaplan, S. Levis, et al. 2003. Evaluation of ecosystem dynamics, plant geography and terrestrial carbon cycling in the LPJ dynamic global vegetation model. *Global Change Biology,* 9**:** 161-185. DOI: 10.1046/j.1365-2486.2003.00569.x

Smith, J. A. C., and H. Griffiths. 1993. *Water Deficits: Plant Responses from Cell to Community* Oxford: Bios Scientific Publishers.

Sood, A., S. A. Prathapar, and V. Smakhtin. 2014. Green and Blue Water. In *Key concepts in water resource management: a review and critical evaluation,* ed. J. Lautze, 91-102 pp. Abingdon, New York: Routledge.

Spracklen, D. V., S. R. Arnold, and C. M. Taylor. 2012. Observations of increased tropical rainfall preceded by air passage over forests. *Nature,* 489**:** 282–285. DOI: 10.1038/nature11390

Staver, A. C., S. Archibald, and S. A. Levin. 2011. The Global Extent and Determinants of Savanna and Forest as Alternative Biome States. *Science,* 334**:** 230-232. DOI: 10.1126/science.1210465

Steffen, W., W. Broadgate, L. Deutsch, O. Gaffney, and C. Ludwig. 2015a. The trajectory of the Anthropocene: The Great Acceleration. *The Anthropocene Review,* 2**:** 81-98. DOI: 10.1177/2053019614564785

Steffen, W., Å. Persson, L. Deutsch, J. Zalasiewicz, M. Williams, K. Richardson, C. Crumley, P. Crutzen, et al. 2011. The Anthropocene: From Global Change to Planetary Stewardship. *Ambio,* 40**:** 739-761. DOI: 10.1007/s13280-011-0185-x

Steffen, W., K. Richardson, J. Rockström, S. E. Cornell, I. Fetzer, E. M. Bennett, R. Biggs, S. R. Carpenter, et al. 2015b. Planetary boundaries: Guiding human development on a changing planet. *Science,* 347**:** 1259855-1259855. DOI: 10.1126/science.1259855

Steffen, W., A. Sanderson, and P. D. Tyson. 2004. *Global Change and the Earth System: A Planet Under Pressure*. Berlin, Heidelberg, New York: Springer-Verlag.

Sterling, S. M., A. Ducharne, and J. Polcher. 2012. The impact of global land-cover change on the terrestrial water cycle. *Nature Climate Change,* 3**:** 385-390. DOI: 10.1038/nclimate1690

Swift Jr., L. W., W. T. Swank , J. B. Mankin, R. J. Luxmoore, and R. A. Goldstein. 1975. Simulation of evapotranspiration and drainage from mature and clear-cut deciduous forests and young pine plantation. *Water Resources Research,* 11**:** 667-673. DOI: 10.1029/WR011i005p00667

Tyree, M. T. 1997. The Cohesion-Tension theory of sap ascent: current controversies. *Journal of Experimental Botany,* 48**:** 1753-1765.

van der Ent, R. J., H. H. G. Savenije, B. Schaefli, and S. C. Steele-Dunne. 2010. Origin and fate of atmospheric moisture over continents. *Water Resources Research,* 46. DOI: 10.1029/2010wr009127

van der Ent, R. J., L. Wang-Erlandsson, P. W. Keys, and H. H. G. Savenije. 2014. Contrasting roles of interception and transpiration in the hydrological cycle – Part 2: Moisture recycling. *Earth System Dynamics,* 5**:** 471-489. DOI: 10.5194/esd-5-471-2014

Vörösmarty, C. J., P. Green, J. Salisbury, and R. B. Lammers. 2000. Global water resources: Vulnerability from climate change and population growth. *Science,* 289**:** 284-288. DOI: 10.1126/science.289.5477.284

Wagner, W., K. Scipal, and C. Pathe. 2003. Evaluation of the agreement between the first global remotely sensed soil moisture data with model and precipitation data. *Journal of Geophysical Research,* 108. DOI: 10.1029/2003jd003663

Weng, W., M. K. B. Luedeke, D. C. Zemp, T. Lakes, and J. P. Kropp. 2018. Aerial and surface rivers: downwind impacts on water availability from land use changes in Amazonia. *Hydrology and Earth System Sciences,* 22**:** 911-927. DOI: 10.5194/hess-22-911-2018

Zemp, D. C., C. F. Schleussner, H. M. Barbosa, M. Hirota, V. Montade, G. Sampaio, A. Staal, L. Wang-Erlandsson, et al. 2017. Self-amplified Amazon forest loss due to vegetation-atmosphere feedbacks. *Nature Communications,* 8**:** 14681. DOI: 10.1038/ncomms14681

Zhang, T., X. Zhang, D. Xia, and Y. Liu. 2014. An Analysis of Land Use Change Dynamics and Its Impacts on Hydrological Processes in the Jialing River Basin. *Water,* 6**:** 3758-3782. DOI: 10.3390/w6123758

Zickfeld, K., B. Knopf, V. Petoukhov, and H. Schellnhuber. 2005. Is the Indian summer monsoon stable against global change? *Geophysical Research Letters,* 32**:** L15707. DOI: 10.1029/2005GL022771

Appendix

Appendix A: Complete list of applied PFTs and CFTs 42
Appendix B: Productive GW-flow maps 43
Appendix C: Unproductive GW-flow maps 44
Appendix D: Global runoff maps 46
Appendix E: Global discharge maps 47
Appendix F: Change of percental PFT coverage 48
Appendix G: Additional regional plots 48

Appendix A: Complete list of applied PFTs and CFTs

The 11 Plant functional types (PFTs) in LPJmL

Abbreviation	*Definition*	*Additional description*
TrBE	Tropical broadleaved evergreen tree	
TrBR	Tropical broadleaved raingreen tree	
TeNE	Temperate needle-leaved evergreen tree	
TeBE	Temperate broadleaved evergreen tree	
TeBS	Temperate broadleaved summergreen tree	
BoNE	Boreal needle-leaved evergreen tree	
BoSE	Boreal broadleaved summergreen tree	
BoNS	Boreal needle-leaved summergreen tree	
TrH	Tropical herbaceous (C4)	
TeH	Temperate herbaceous (C3)	
PoH	Polar herbaceous (C3)	

The 16 CFTs (incl. 2 Bioenergy functional types) in LPJmL

Abbreviation	*Definition*	*Additional description*
TeCer	Temperate cereals	wheat, rye, barley
Rice	Rice	paddy rice; rice
Maize	Maize	maize for food; maize
TrCer	Tropical cereals	millet, sorghum
Pul	Pulses	pulses; field peas
TeRo	Temperate roots	sugar beet
TrRo	Tropical roots	cassava

SunFl	Sunflower	sunflower
Soy	Soybean	soybean
GrNu	Groundnut	groundnuts
Rape	Rapeseed	rapeseed
SuCa	Sugarcane	sugarcane
	Others	potatoes, oil palm, citrus, date palm, grapes, cotton, cocoa, coffee, pastures, managed grasslands
	Managed grasslands	
	Bio-energy grass	
	Bio-energy grasslands	

Appendix B: Productive GW-flow maps

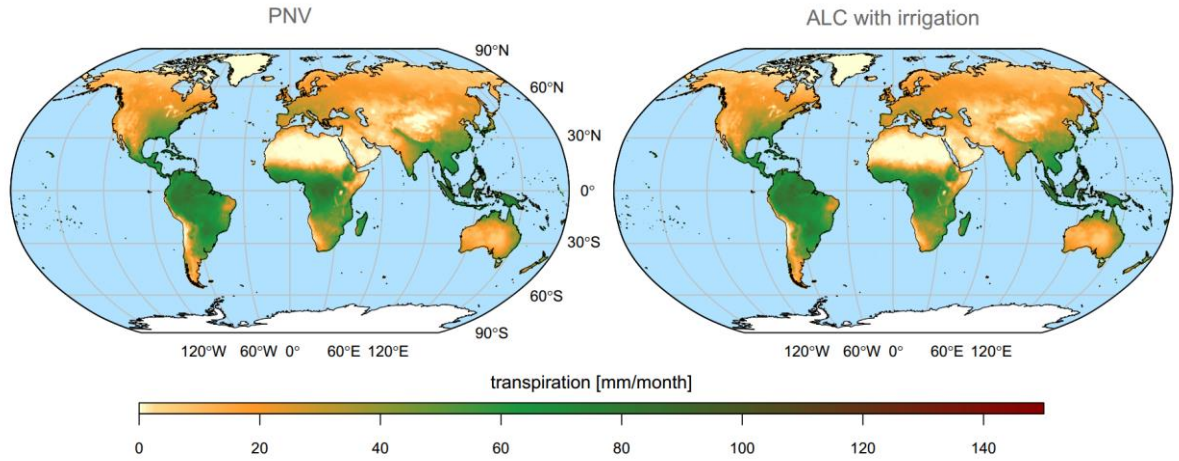

Global monthly transpiration (productive GW-flow) maps representing the average over all months of the last 30 years of the simulation period for a) the PNV run (on the left) and b) the ALC run incorporating irrigation schemes (on the right).

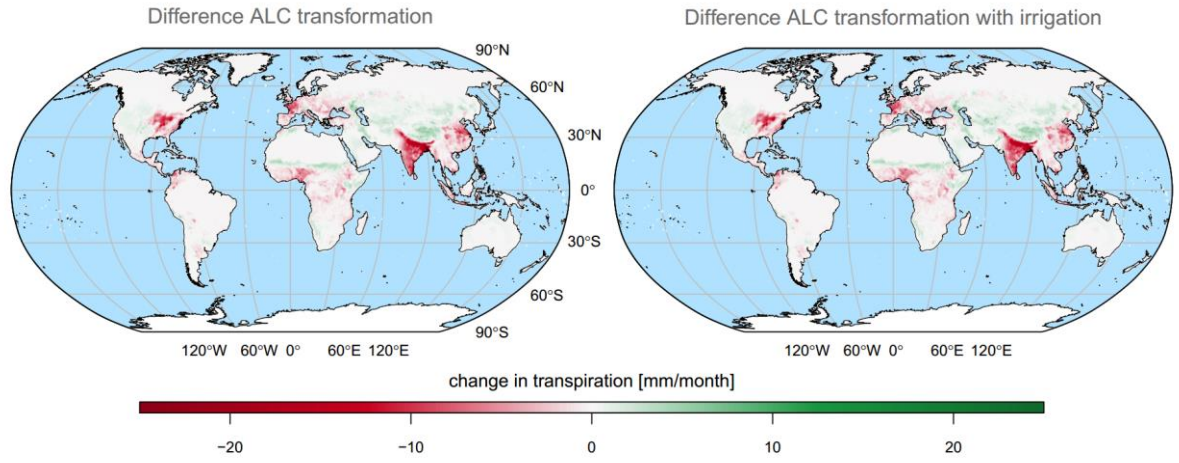

Global monthly transpiration (productive GW-flow) difference maps representing the average changes in transpiration over all months of the last 30 years of the simulation period. Whilst areas in red show a decline in transpiration, areas in green show an increase as a consequence of the ALC conversion a) without irrigation schemes and b) with irrigation schemes.

Appendix C: Unproductive GW-flow maps

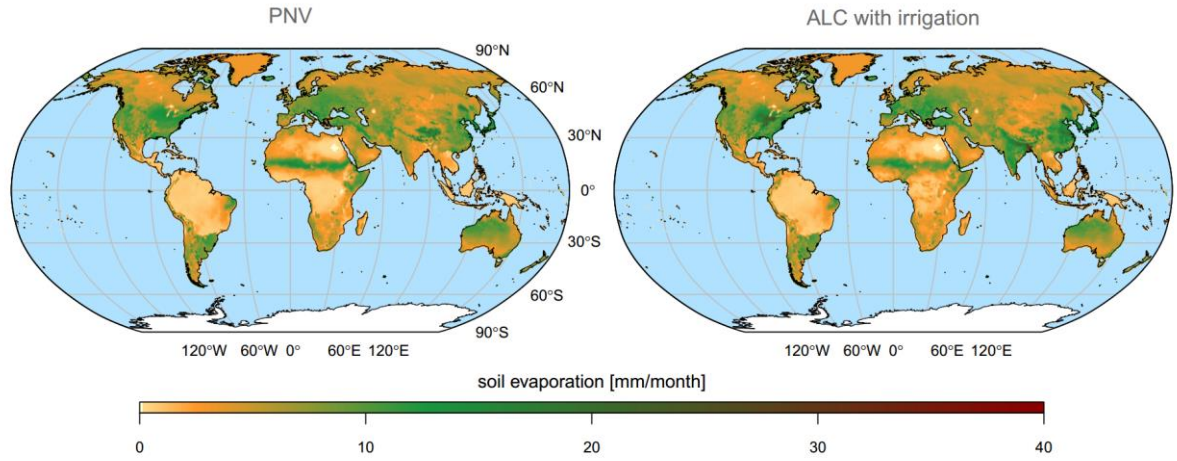

Global monthly soil evaporation (unproductive GW-flow) maps representing the average over all months of the last 30 years of the simulation period for a) the PNV run (on the left) and b) the ALC run incorporating irrigation schemes (on the right).

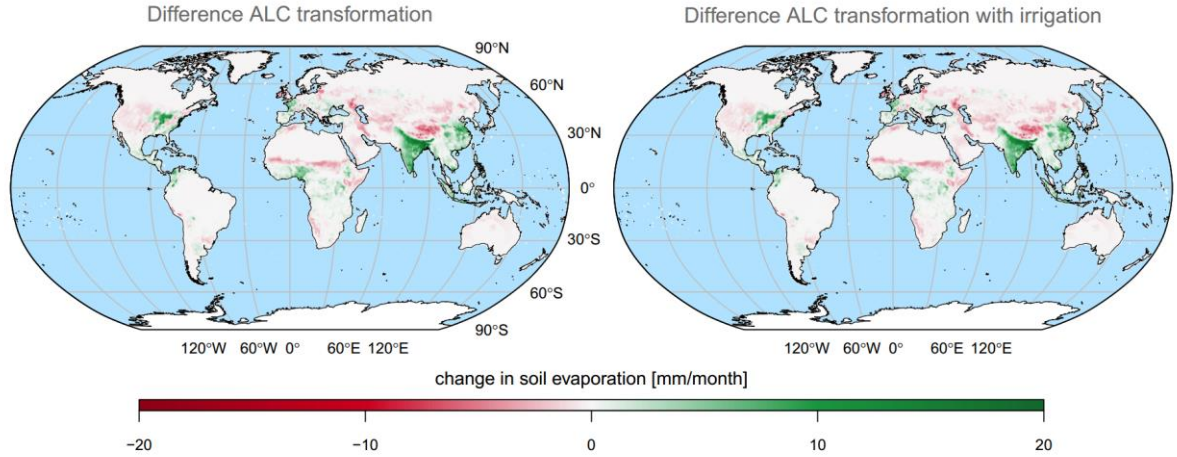

Global monthly soil evaporation (unproductive GW-flow) difference maps representing the average changes in soil evaporation over all months of the last 30 years of the simulation period. Whilst areas in red show a decline in soil evaporation, areas in green show an increase as a consequence of the ALC conversion a) without irrigation schemes and b) with irrigation schemes.

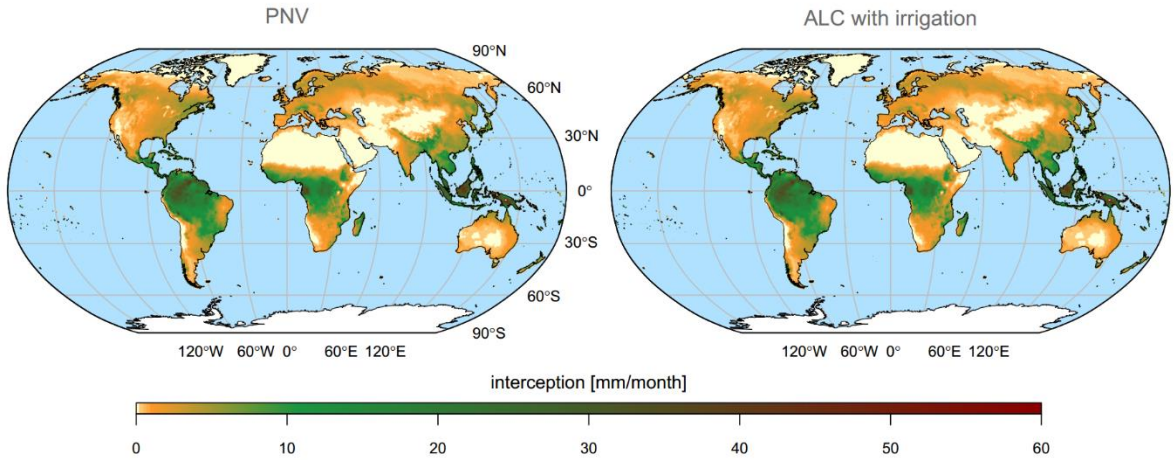

Global monthly interception (unproductive GW-flow) maps representing the average over all months of the last 30 years of the simulation period for PNVr (on the left) and ALCr_irr (on the right).

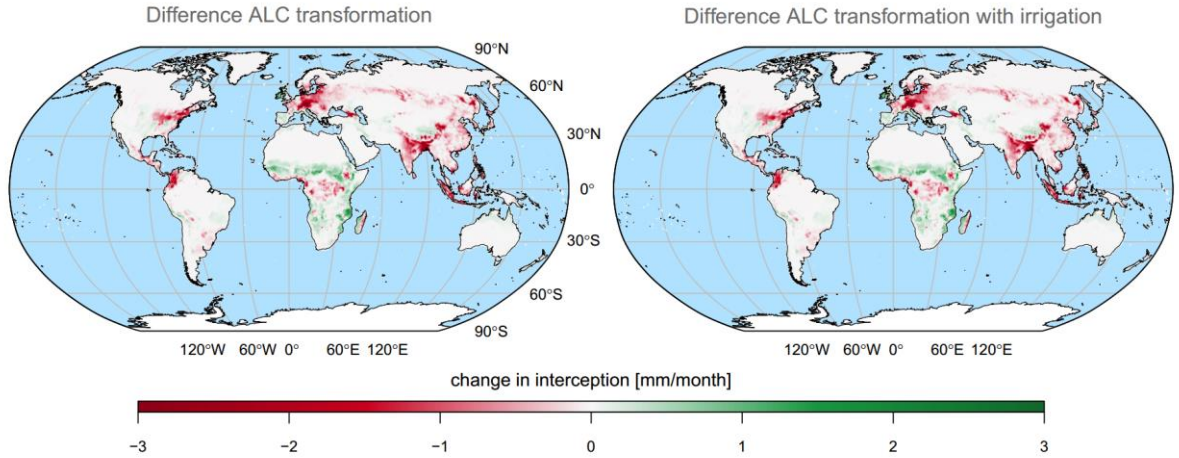

Global monthly interception (unproductive GW-flow) difference maps representing the average changes in interception over all months of the last 30 years of the simulation period. Whilst areas in red show a decline in interception, areas in green show an increase. Difference between PNVr and ALCr on the left and PNVr and ALCr_irr on the right.

Appendix D: Global runoff maps

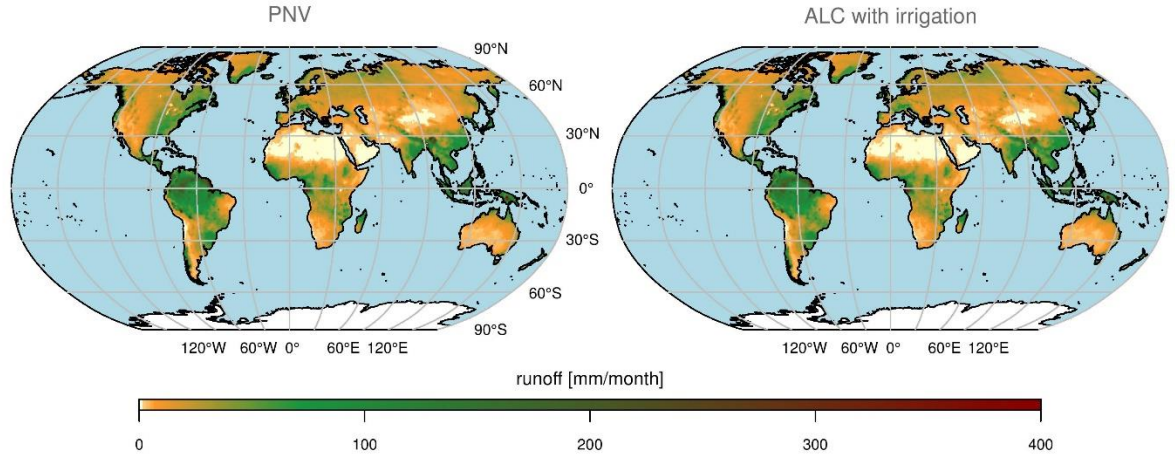

Global monthly runoff maps representing the average over all months of the last 30 years of the simulation period for PNVr (on the left) and ALCr_irr (on the right).

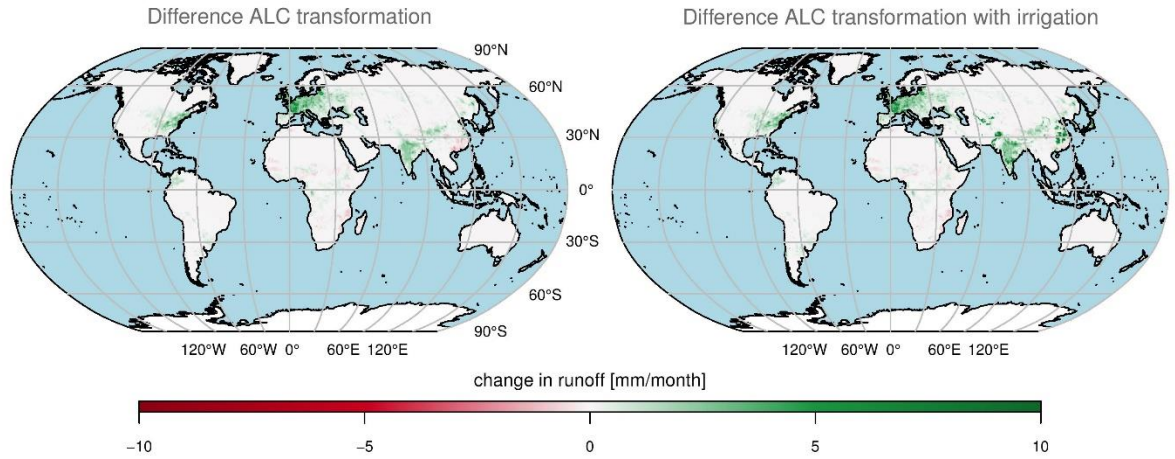

Global monthly runoff difference maps representing the average changes in runoff over all months of the last 30 years of the simulation period. Whilst areas in red show a decline in runoff, areas in green show an increase. Difference between PNVr and ALCr on the left and PNVr and ALCr_irr on the right.

Appendix E: Global discharge maps

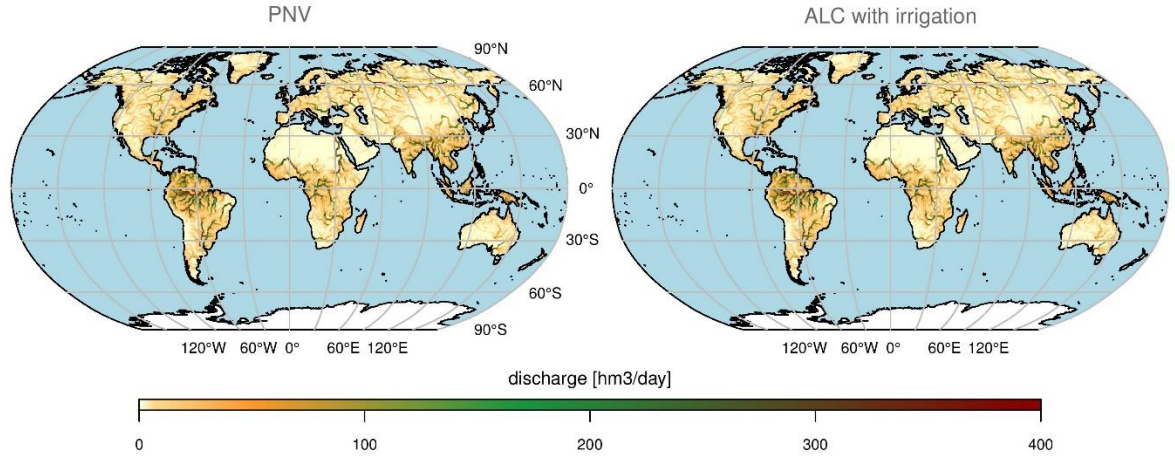

Global monthly discharge maps representing the average over all months of the last 30 years of the simulation period for PNVr (on the left) and ALCr_irr (on the right).

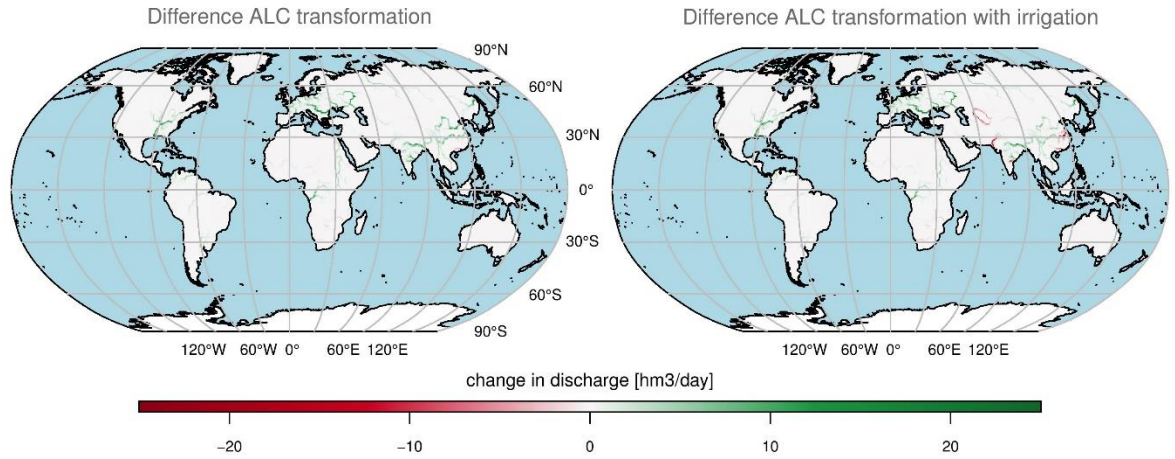

Global monthly discharge difference maps representing the average changes in discharge over all months of the last 30 years of the simulation period. Whilst areas in red show a decline in discharge, areas in green show an increase. Difference between PNVr and ALCr on the left and PNVr and ALCr_irr on the right.

Appendix F: Change of percental PFT coverage

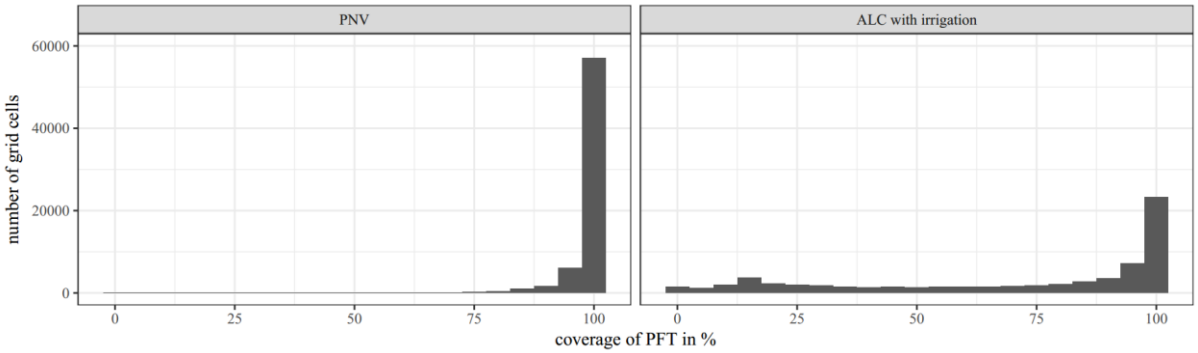

Percental coverage of PFT within each grid cell for both PNVr (on the left) and ALCr_irr (on the right).

Appendix G: Additional regional plots

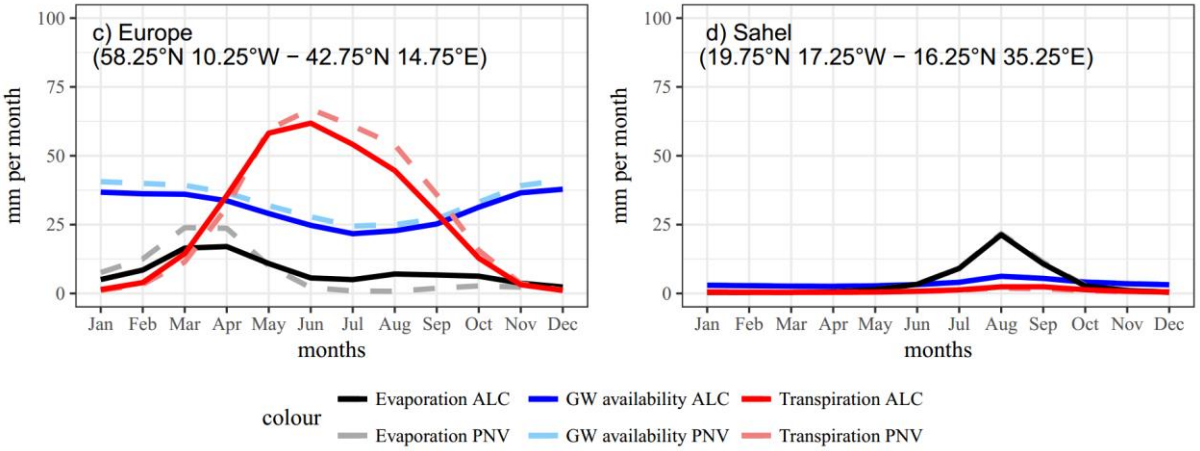

Intra-annual trends of GW_{avail}, E_{soil} and E_{transp} for PNVr and ALCc_irr in c) Europe and d) the Sahel. For the matter of clarity, only the mean values of the 30-year timeframe (1976-2005) were plotted, leaving out the interannual variability